Diagnostics of flow dependent background error statistics with a regional ensemble 3D-var (continuation)

Maria Monteiro*

September 22, 2009

Contents

1 Summary

The present report notes the main activities occured during a 8 weeks stay at Météo-France as part of the ALADIN NWP Project's annual plan for the cooperative development of the ALADIN NWP system. This contribution was splitted in two parts, distributed by two time periods during the months of June/July and September, and was supported by the project flat-rate funds.

*Instituto de Meteorologia, Lisbon, Portugal

The goal of this stay was the progress on the study of the flow dependent background error statistics estimated by a regional 3D-var ensemble system following the work started in 2008. The covariances of model parameters as well as its cross-covariances with control variables estimated by the ALADIN/France 6 member ensemble system were analysed for two periods of 30 days, one during Winter and one during Summer. The first part of the results (univariate) as well as the verified conclusions were organised under a scientific article whose text is now being reviewed. Meanwhile results analysis also started for the second set of statistics (multivariate) which are now being organised as a second scientific article that should be reviewed later on.

The univariate part of this study derived the conclusion that the estimated covariances show seasonal variations, as well as day-to-day variations according with the weather situation. Moreover, for the lower layers of the troposphere it was shown that significative variations could happen along the diurnal cycle, specially during the Summer period. Generally speaking, it was possible to verify that the error variance increases from Winter to Summer, from synoptic stable to unstable conditions and with the increase of thermal instability on the PBL (in particular with the sunrise), although this rule could not be applied in very particular weather situations. In particular, we could see that, during Winter, the error values on the cyclonic unstable situations are much larger that on the anticyclonic stable cases, typically by a factor of 1.5 for temperature and by a factor of 2.5 for vorticity. Finally, it was verified that these flow-dependent variance estimates were robust, by comparing values provided by two independent 6-member ensembles.

In order to perform the multivariate part of this study, the application "festat" was executed for the two 30 days periods using the flag "lstabal=.true." and for that a new set of 4 experiments with the names "B13A", "B136", "B137", "B138" was created under OLIVE[1]. Up to now, no conclusions have been taken for this second set of results - the cross-covariances. However, as an example, preliminary plots for the Winter and the Summer seasons and from a frontal (on the 20080712) to a col configuration (on the 20080723) are here included already as appendix, showing the basic differences on these statistical structures under contrasting weather situations.

As a foreseen progress of this work, impact studies on the use of the performed statistics at the reference data assimilation system should be performed.

[1]Outil de Lancement Interactif et de Visualisation d'Experiences

2 Acknowledgements

Loïk Berre is supervising this study. Acknowledgements are also due to Claude Fischer for interfacing the present cooperation between the Portuguese meteorological service and Météo-France, under the ALADIN NWP project. Moreover, to all the GMAP/CNRM team for their hospitality during my stay in Toulouse. Special thanks are due to Eric Sevault for his support with the OLIVE system and for his companionship. To the Portuguese meteorological services and in particular to the CPPN team for my present time availability to perform this study.

A Seasonal variation of cross-covariances

A.1 Vorticity-divergence couplings

(a) (b)

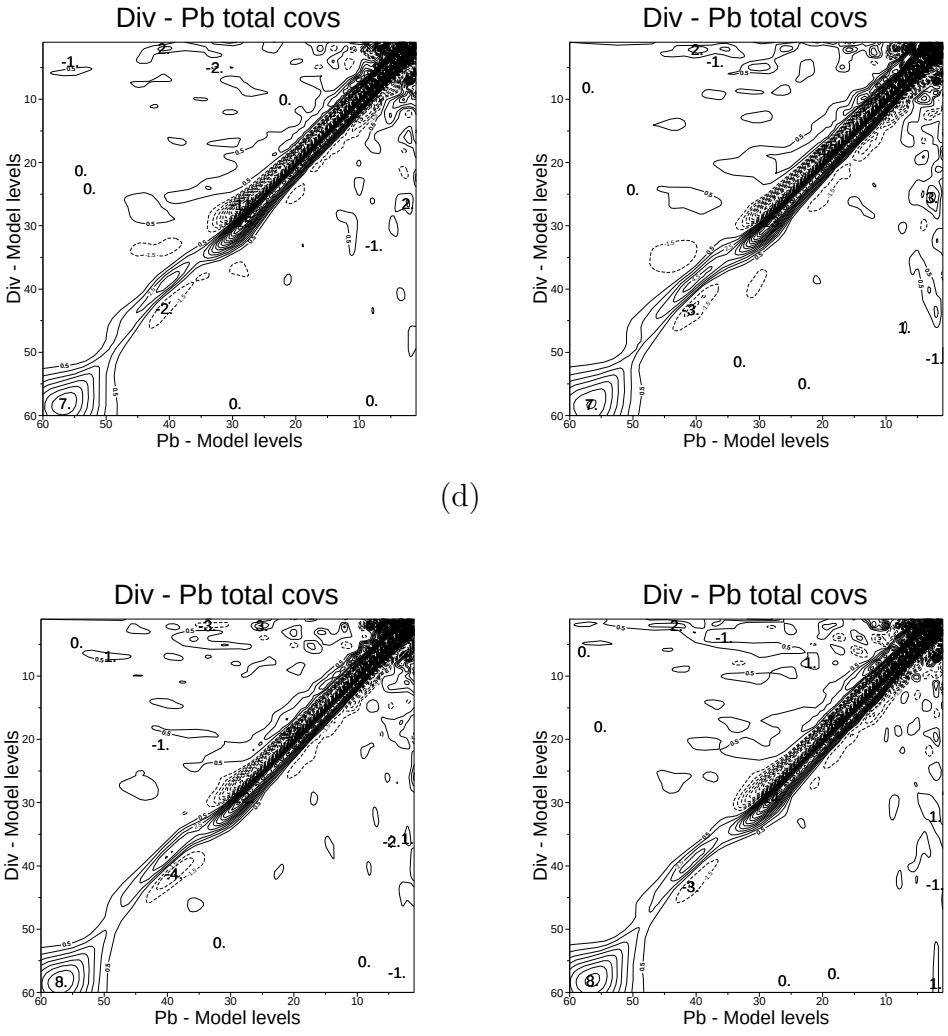

(c) (d)

Figure 1: Mean vertical cross-covariance matrices between divergence and vorticity-balanced geopotential of 6 hour ALADIN/France forecast errors estimated by the second Winter ensemble for the networks: (a) 00UTC, (b) 06UTC, (c) 12UTC and (d) 18UTC.

(a) (b)

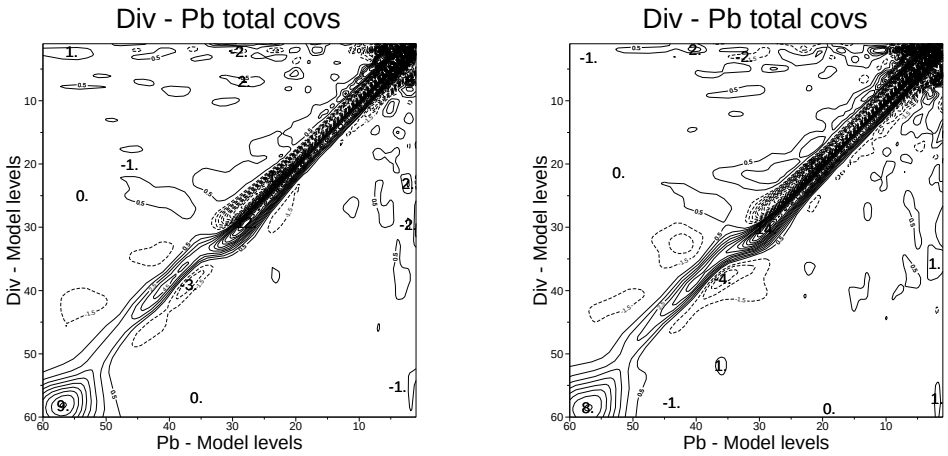

(c) (d)

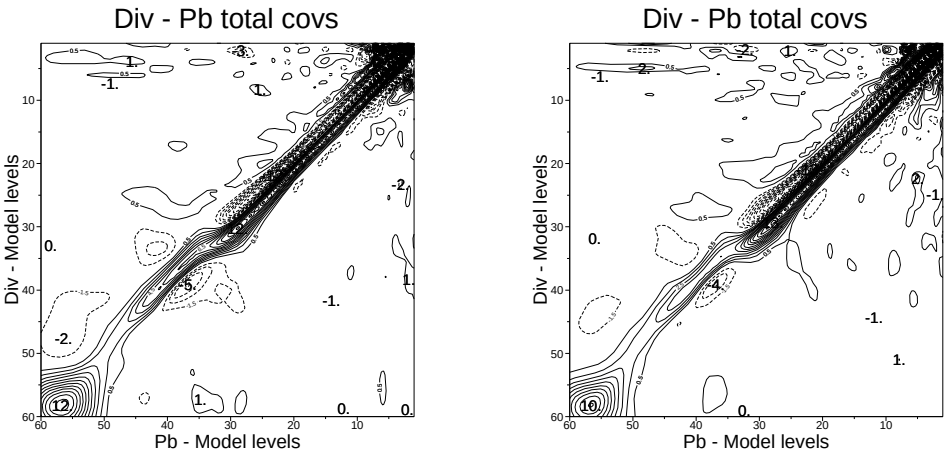

Figure 2: Mean vertical cross-covariance matrices between divergence and vorticity-balanced geopotential of 6 hour ALADIN/France forecast errors estimated by the second Summer ensemble for the networks: (a) 00UTC, (b) 06UTC, (c) 12UTC and (d) 18UTC.

A.2 Mass-wind couplings

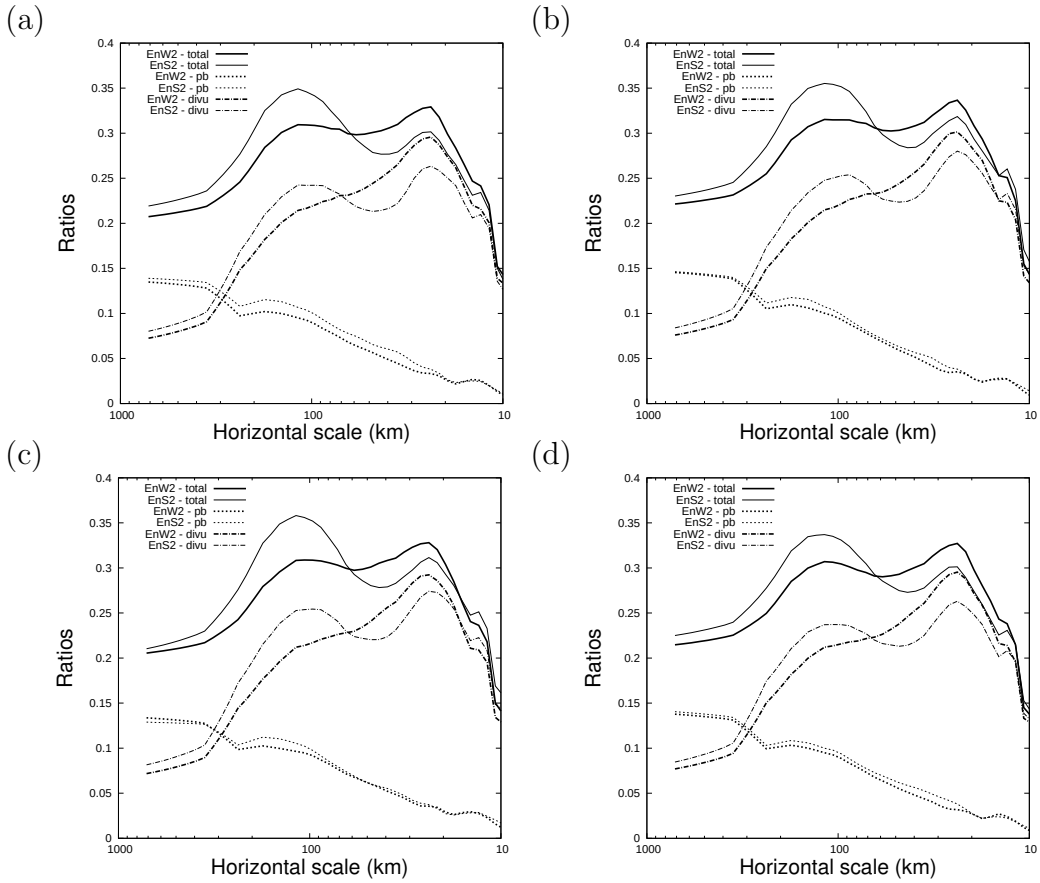

Figure 3: Vertical averages of the percentage of explained temperature variance of 6 hour ALADIN/France forecast errors estimated by the second Winter ensemble as a function of the horizontal scale, for all networks: (a) 00UTC, (b) 06UTC, (c) 12UTC and (d) 18UTC.

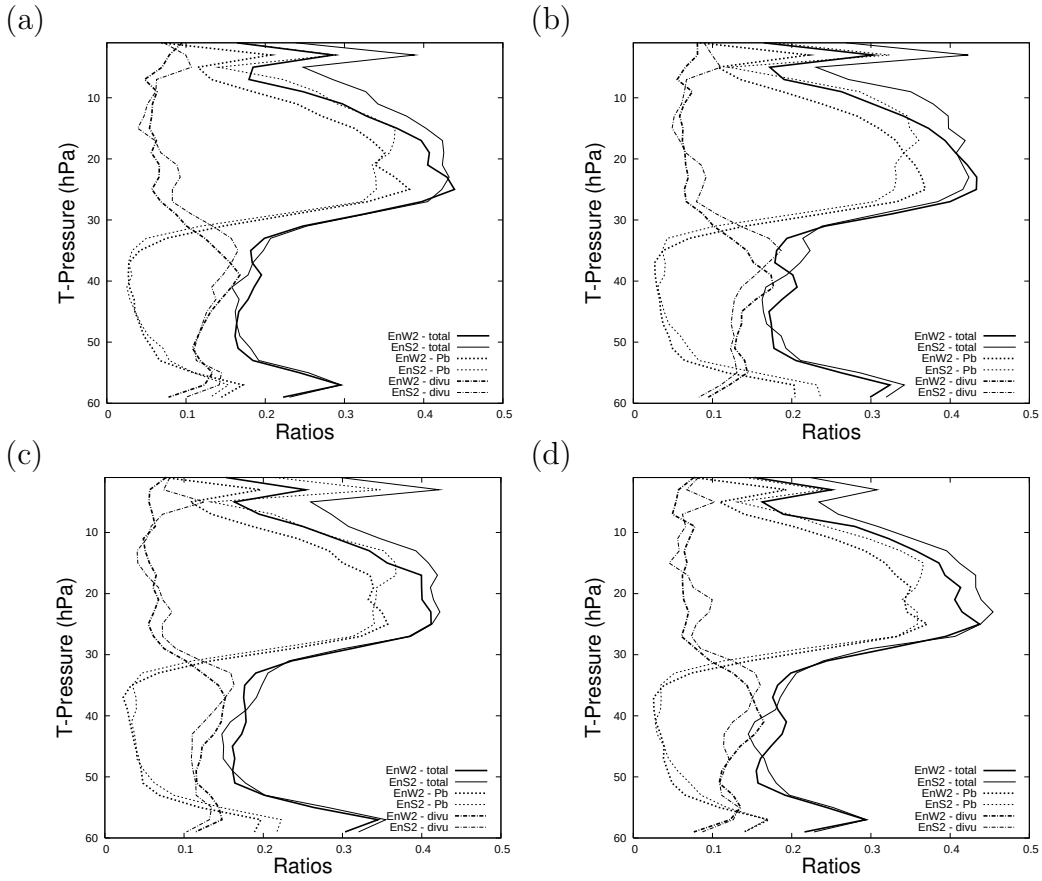

Figure 4: Spectral averages of the percentage of explained temperature variance of 6 hour ALADIN/France forecast errors estimated by the second Winter ensemble as a function of height, for all networks: (a) 00UTC, (b) 06UTC, (c) 12UTC and (d) 18UTC.

(a) (b)

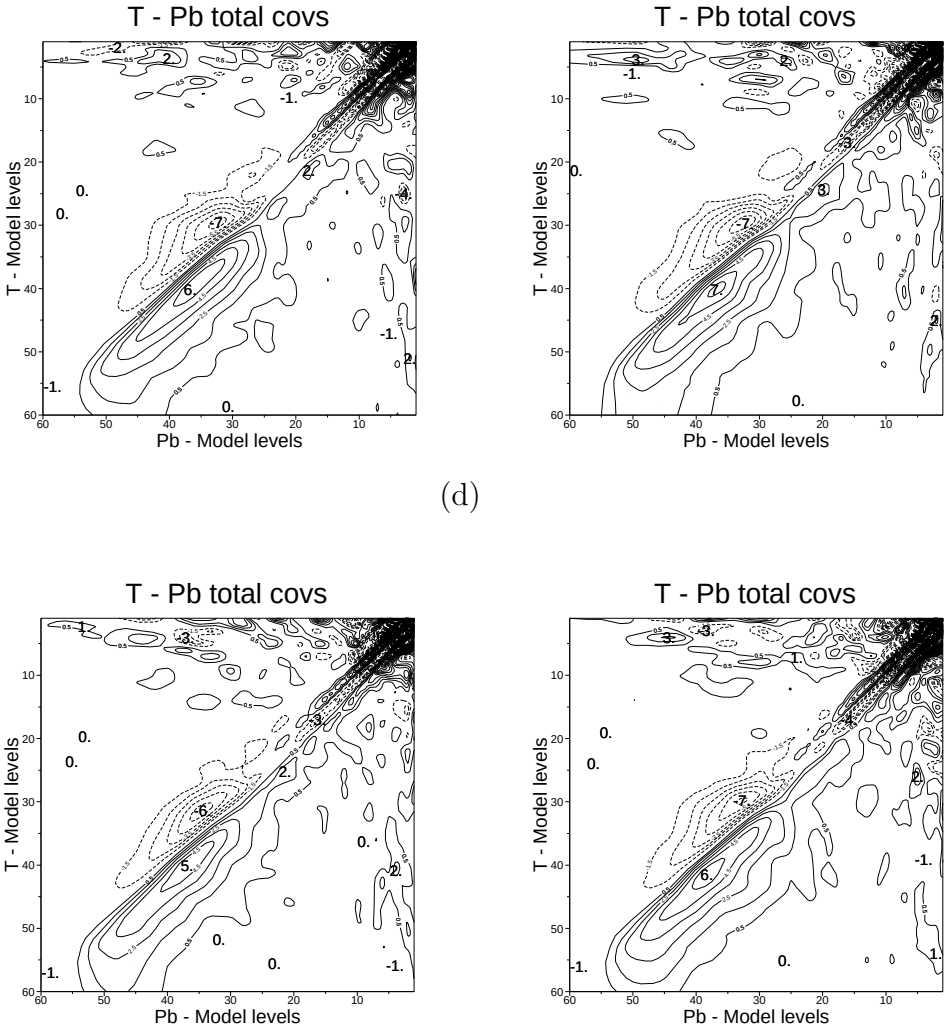

Figure 5: Mean cross-covariances matrices between temperature and balanced geopotential of 6 hour ALADIN/France forecast errors estimated by the second Winter ensemble for all networks: (a) 00UTC, (b) 06UTC, (c) 12UTC and (d) 18UTC.

(a) (b)

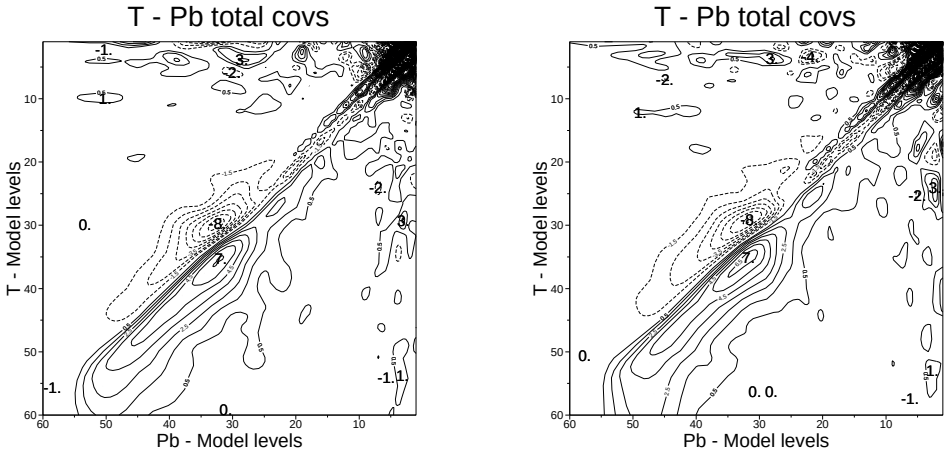

(c) (d)

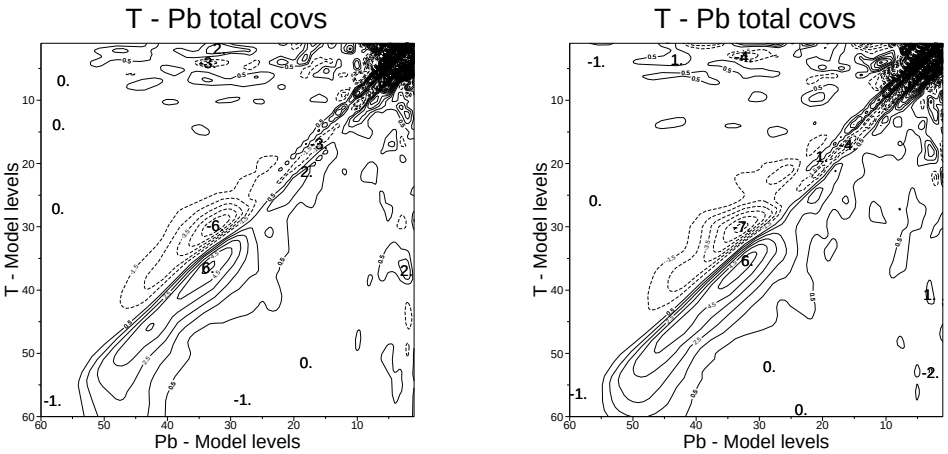

Figure 6: Mean cross-covariances matrices between temperature and balanced geopotential of 6 hour ALADIN/France forecast errors estimated by the second Summer ensemble for all network: (a) 00UTC, (b) 06UTC, (c) 12UTC and (d) 18UTC.

(a) (b)

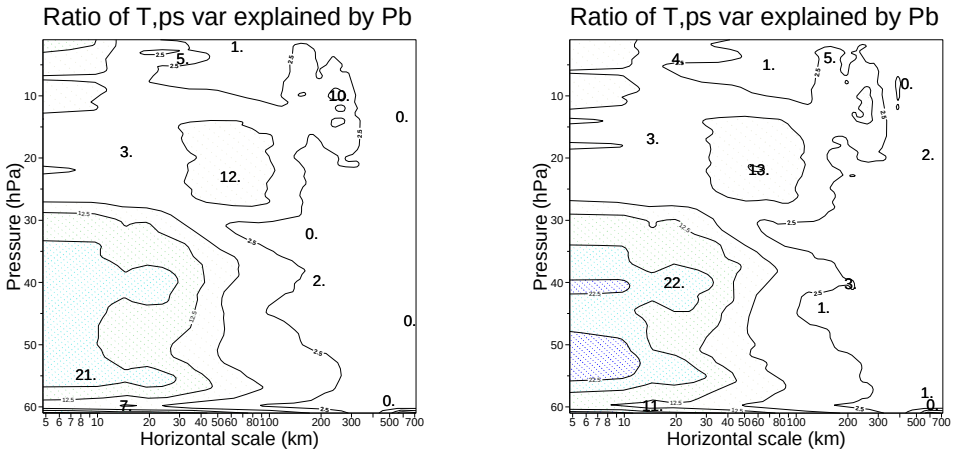

(c) (d)

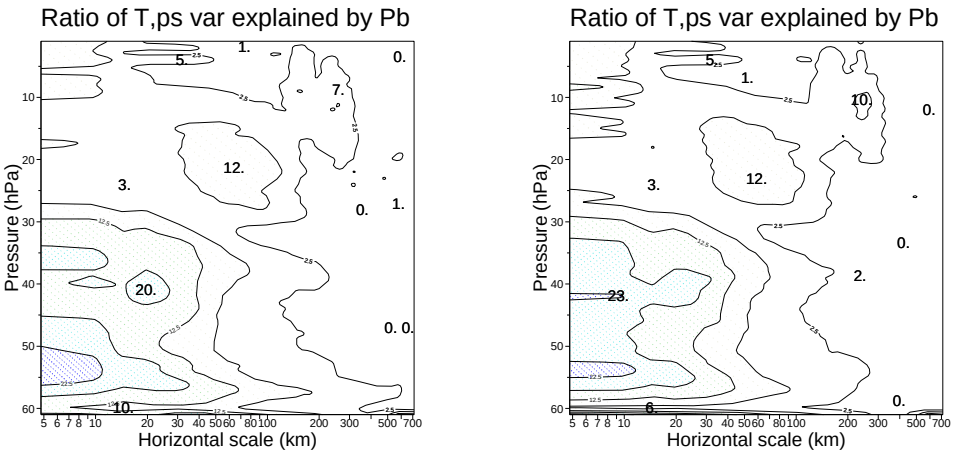

Figure 7: Percentage of the variance of temperature that is explained by balanced geopotential of 6 hour ALADIN/France forecast errors estimated by the second Winter ensemble for all networks: (a) 00UTC, (b) 06UTC, (c) 12UTC and (d) 18UTC.

(a) (b)

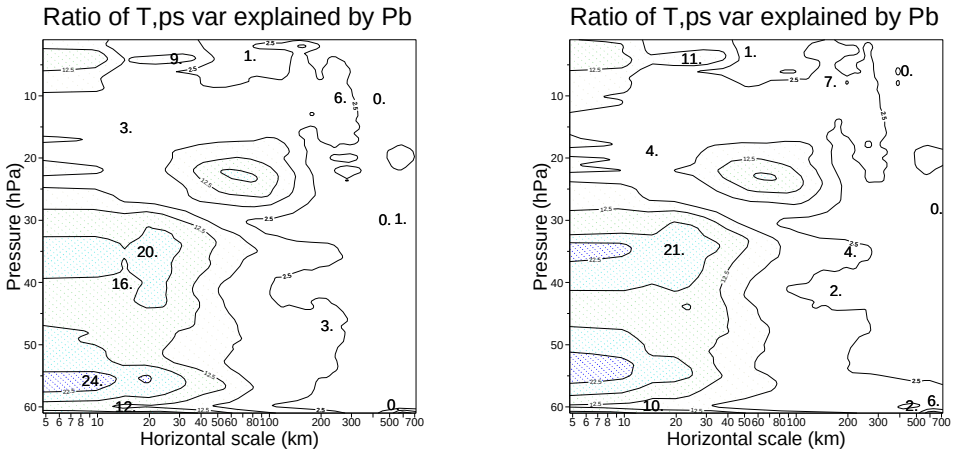

(c) (d)

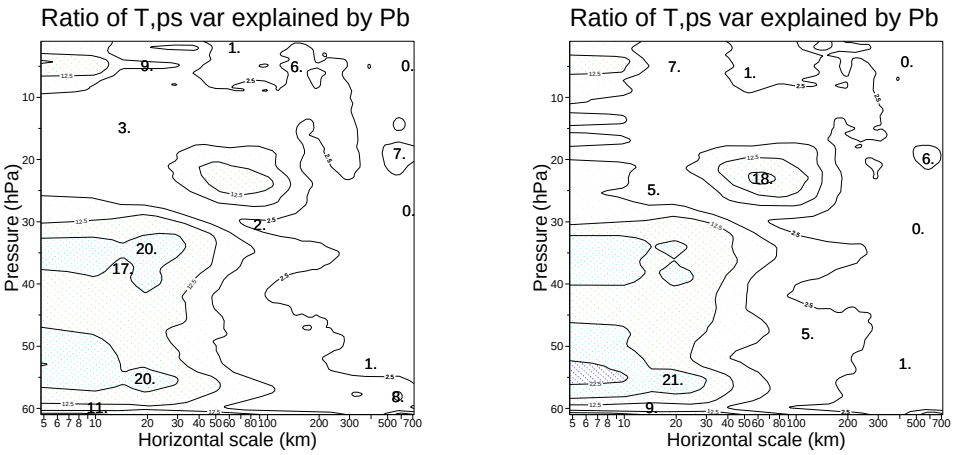

Figure 8: Percentage of the variance of temperature that is explained by balanced geopotential of 6 hour ALADIN/France forecast errors estimated by the second Summer ensemble for all networks: (a) 00UTC, (b) 06UTC, (c) 12UTC and (d) 18UTC.

(a) (b)

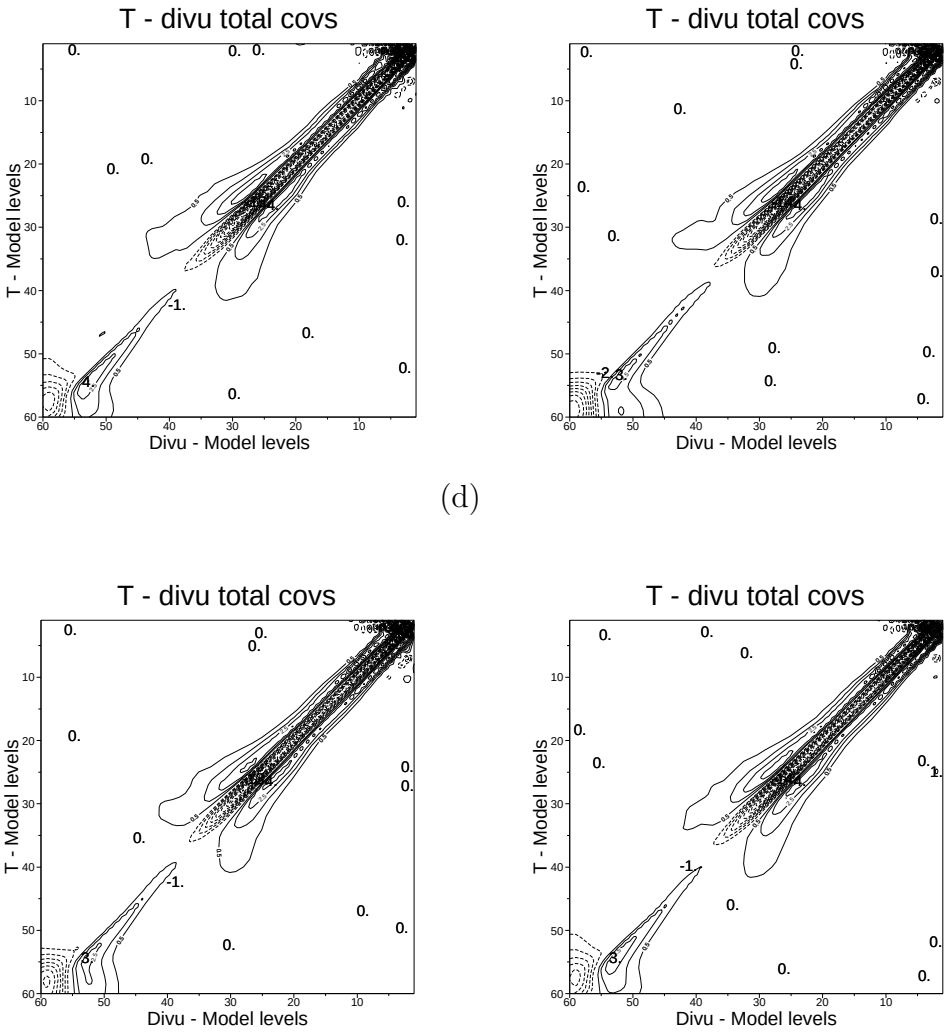

(c) (d)

Figure 9: Mean vertical cross-covariance matrices between temperature and unbalanced divergence of 6 hour ALADIN/France forecast errors estimated by the second Winter ensemble for all the networks: (a) 00UTC, (b) 06UTC, (c) 12UTC and (d) 18UTC.

(a) (b)

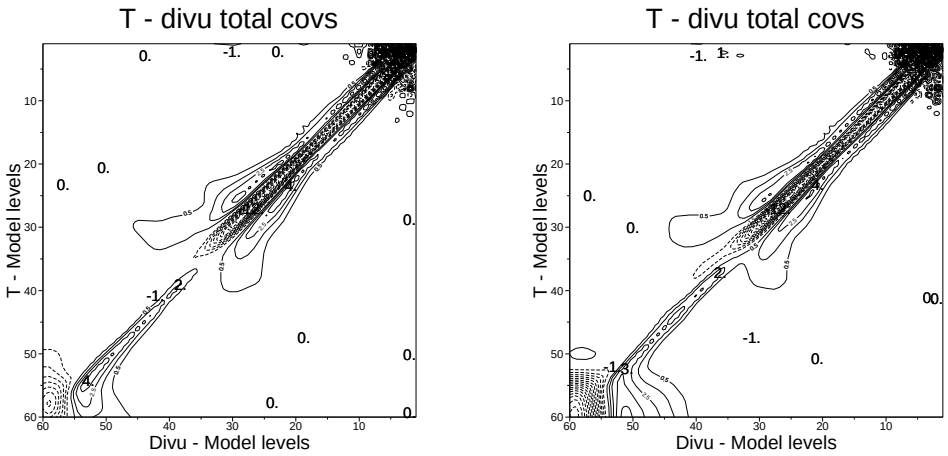

(c) (d)

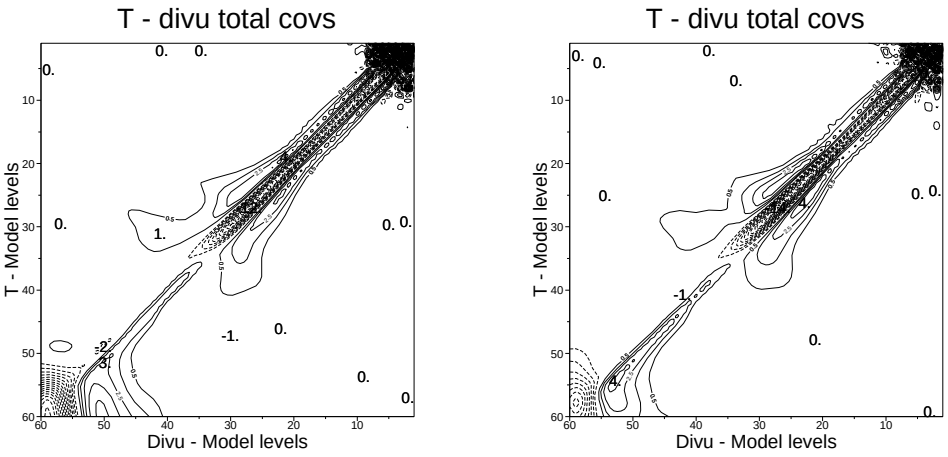

Figure 10: Mean vertical cross-covariance matrix between temperature and unbalanced divergence of 6 hour ALADIN/France forecast errors estimated by the second Summer ensemble for all the networks: (a) 00UTC, (b) 06UTC (c) 12UTC (d) 18UTC.

(a) (b)

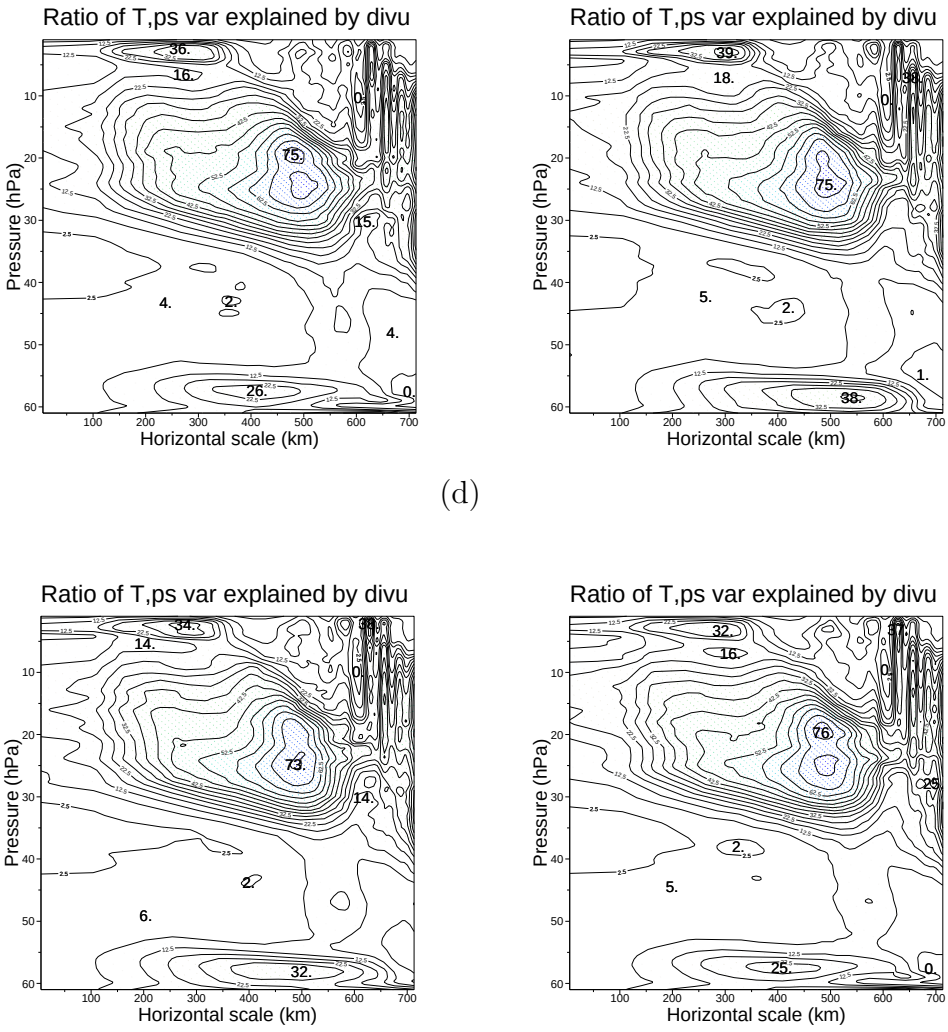

Figure 11: Percentage of the variance of temperature that is explained by the unbalanced divergence of 6 hour ALADIN/France forecast errors estimated by the second Winter ensemble for all the networks: (a) 00UTC, (b) 06UTC, (c) 12UTC and (d) 18UTC.

(a) (b)

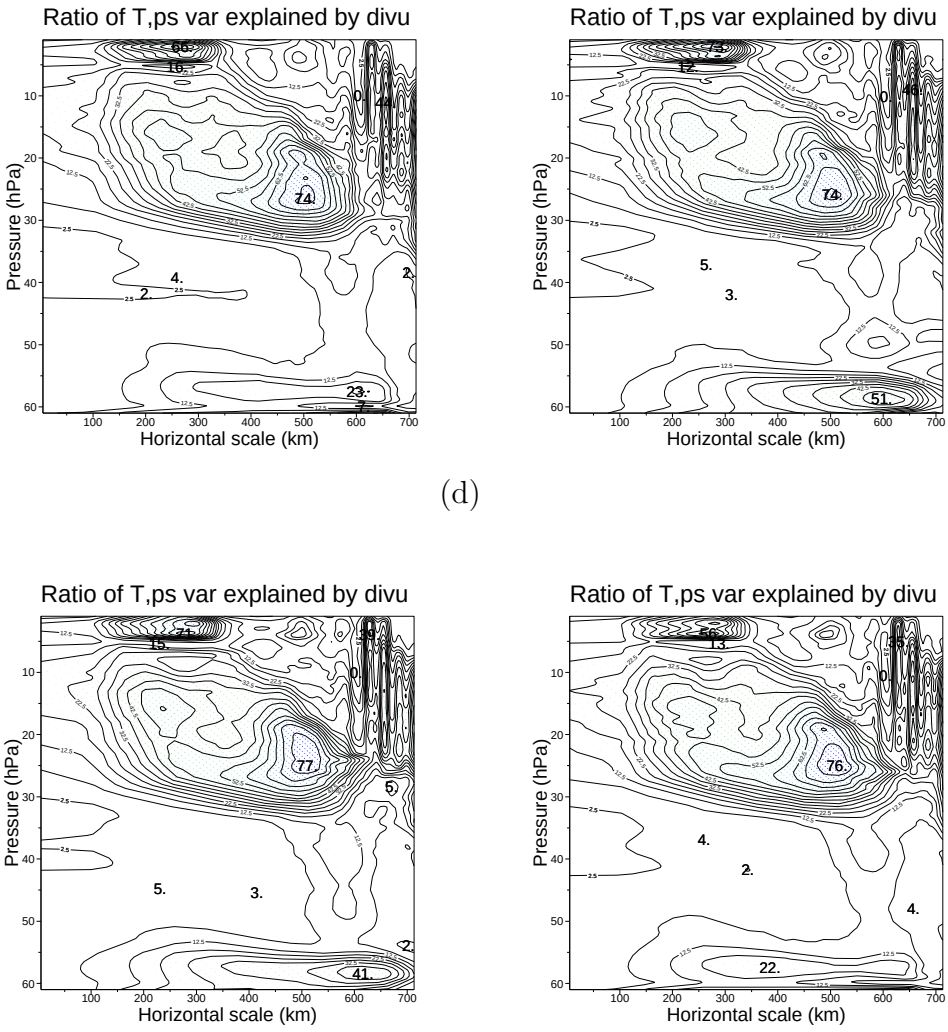

(c) (d)

Figure 12: Mean vertical cross-covariance matrix between temperature and unbalanced divergence of 6 hour ALADIN/France forecast errors estimated by the second Summer ensemble for all the networks: (a) 00UTC, (b) 06UTC (c) 12UTC (d) 18UTC.

A.3 Couplings involving humidity

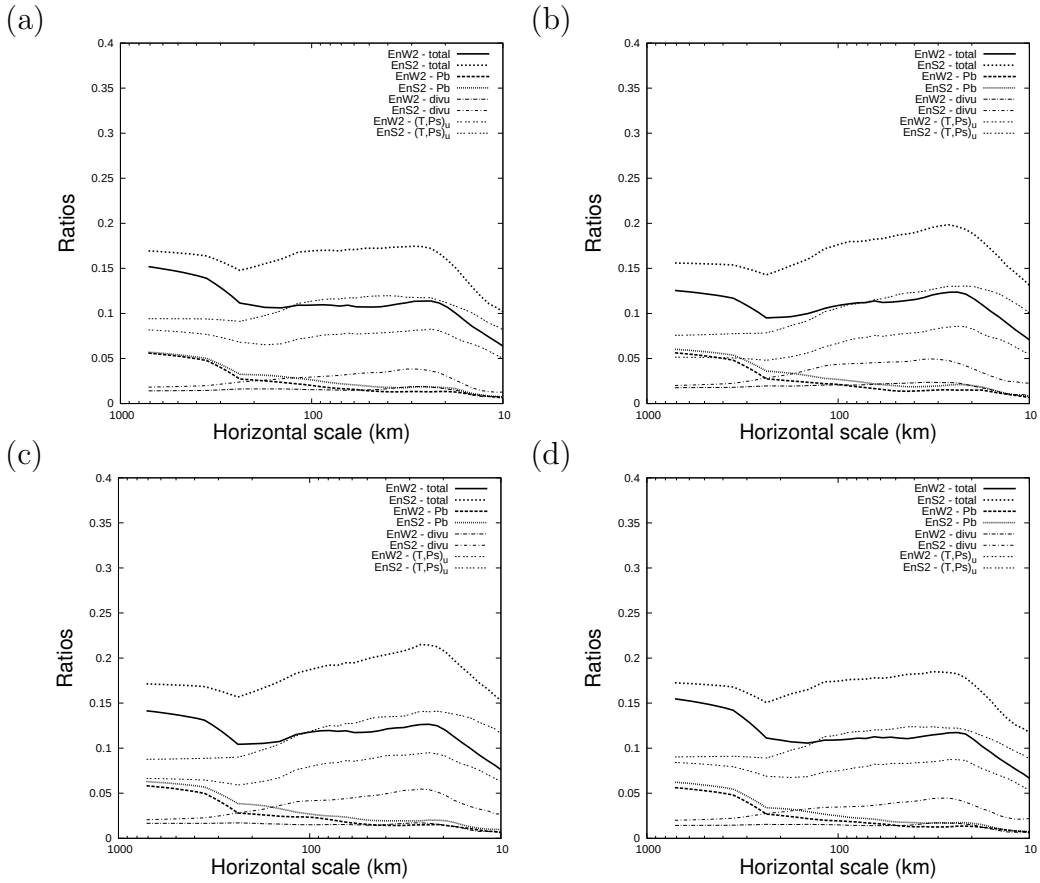

Figure 13: Vertical averages of the percentage of explained temperature variance of 6 hour ALADIN/France forecast errors estimated by the second Winter ensemble, as a function of horizontal scale, for all networks: (a) 00UTC, (b) 06UTC, (c) 12UTC and (d) 18UTC.

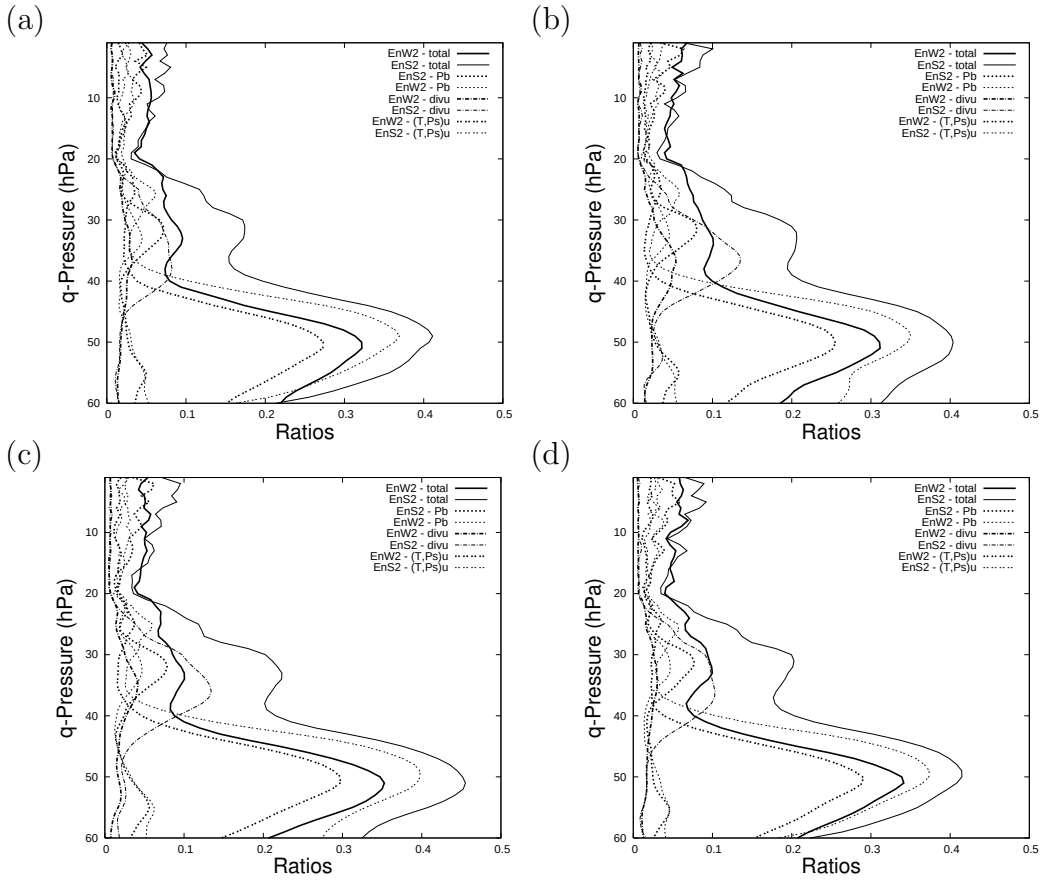

Figure 14: Spectral averages of the percentage of explained temperature variance of 6 hour ALADIN/France forecast errors estimated by the second Winter ensemble, as a function of height, for all networks: (a) 00UTC, (b) 06UTC, (c) 12UTC and (d) 18UTC.

(a) (b)

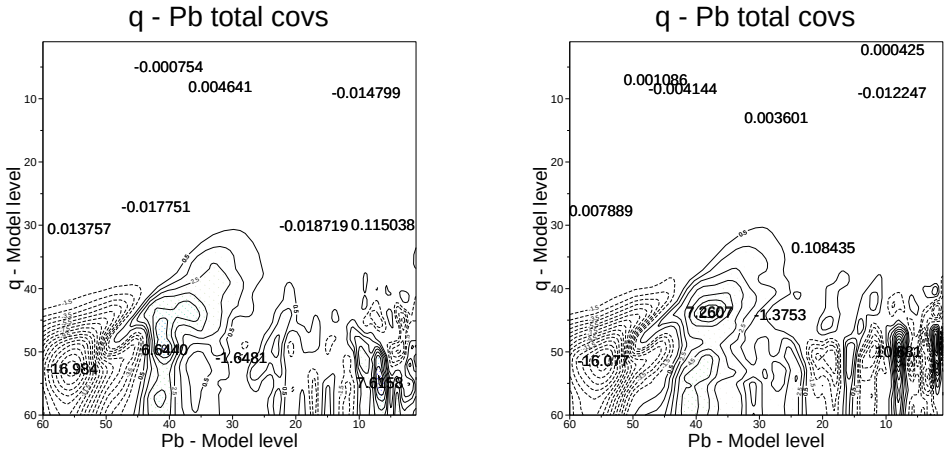

(c) (d)

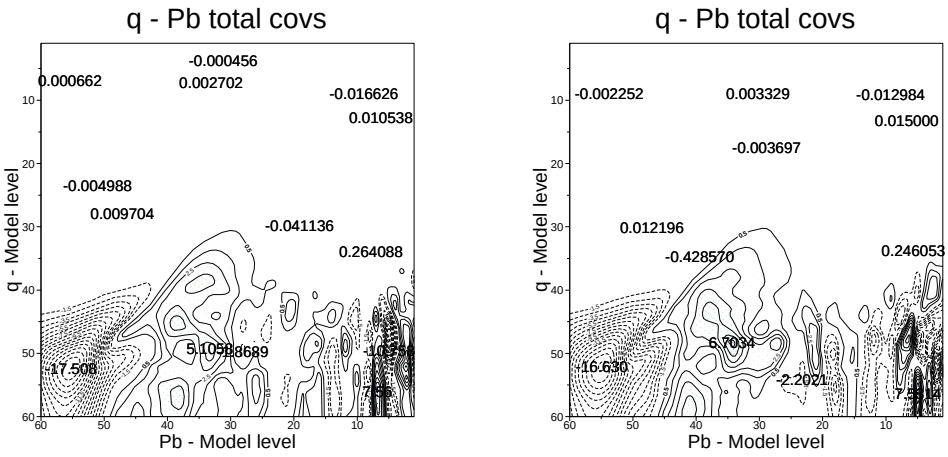

Figure 15: Mean vertical cross-covariance matrices between specific humidity and vorticity-balanced geopotential of 6 hour ALADIN/France forecast errors estimated by the s'econd Winter ensemble for all the networks: (a) 00UTC, (b) 06UTC, (c) 12UTC and (d) 18UTC.

(a) (b)

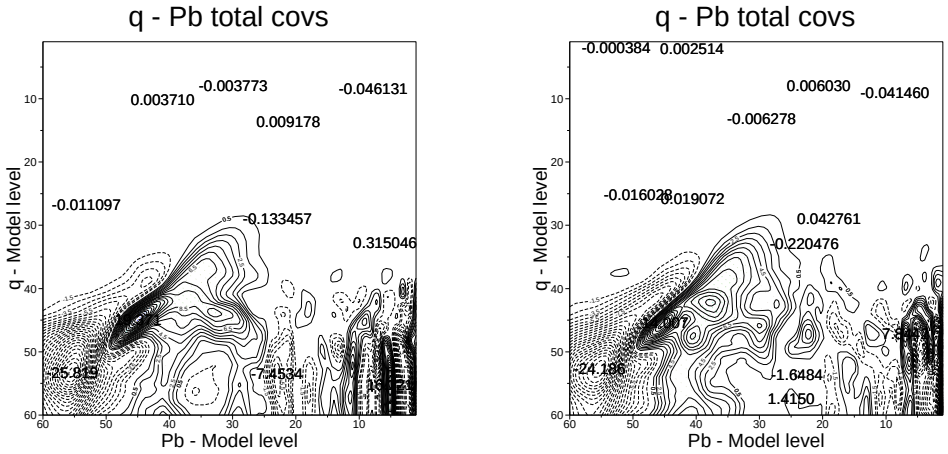

(c) (d)

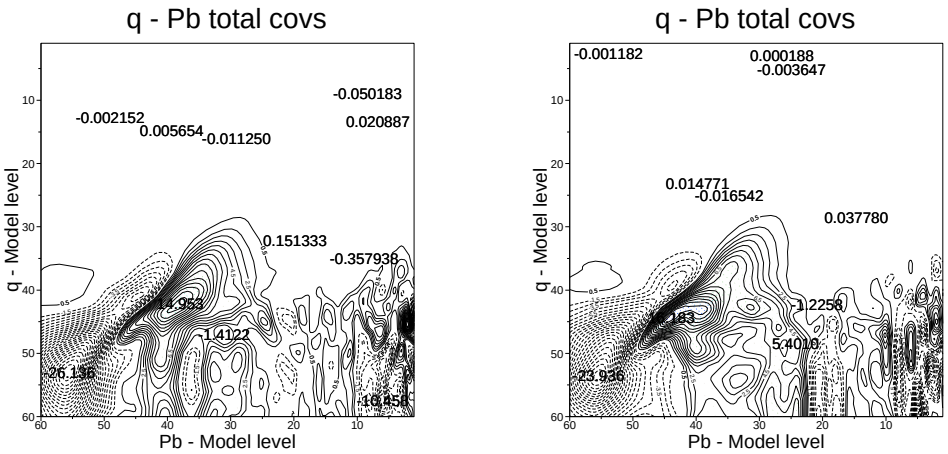

Figure 16: Mean vertical cross-covariance matrices between specific humidity and vorticity-balanced geopotential of 6 hour ALADIN/France forecast errors estimated by the second Summer ensemble for all the networks: (a) 00UTC, (b) 06UTC, (c) 12UTC and (d) 18UTC.

(a) (b)

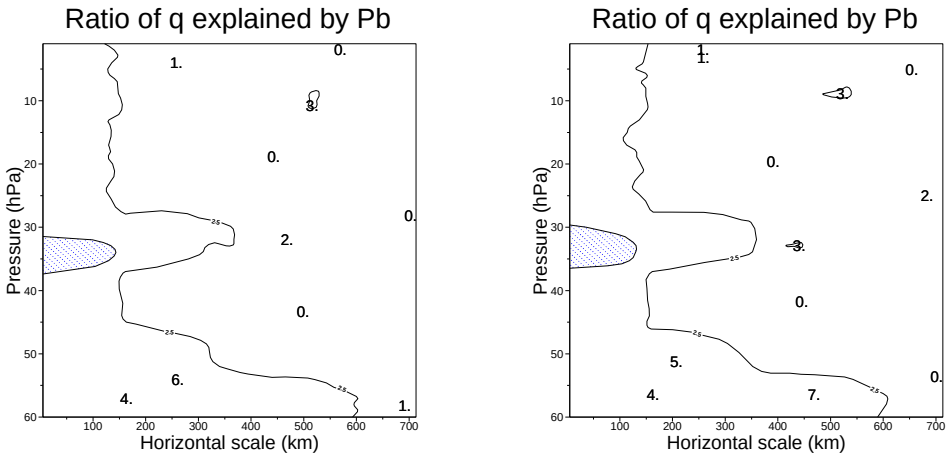

(c) (d)

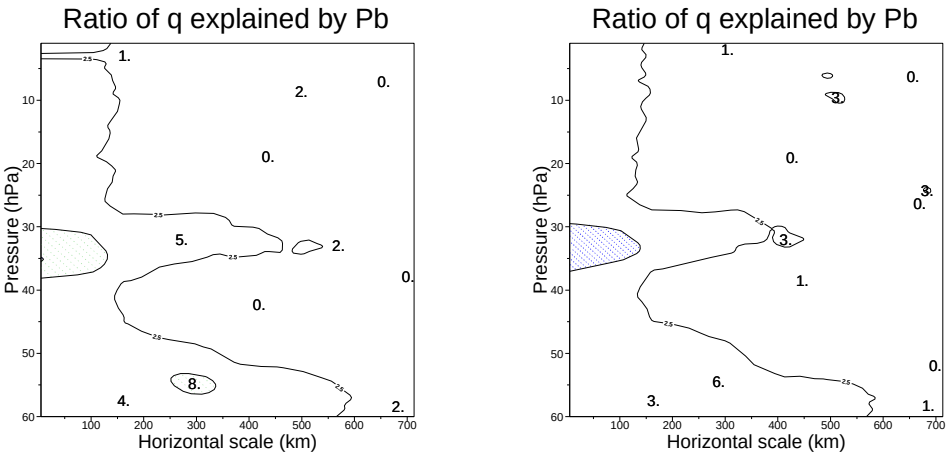

Figure 17: Percentage of the variance of specific humidity that is explained by balanced geopotential of 6 hour ALADIN/France forecast errors estimated by the second Winter ensemble for all networks, for the model parameters: (a) 00UTC, (b) 06UTC, (c) 12UTC and (d) 18UTC.

(a) (b)

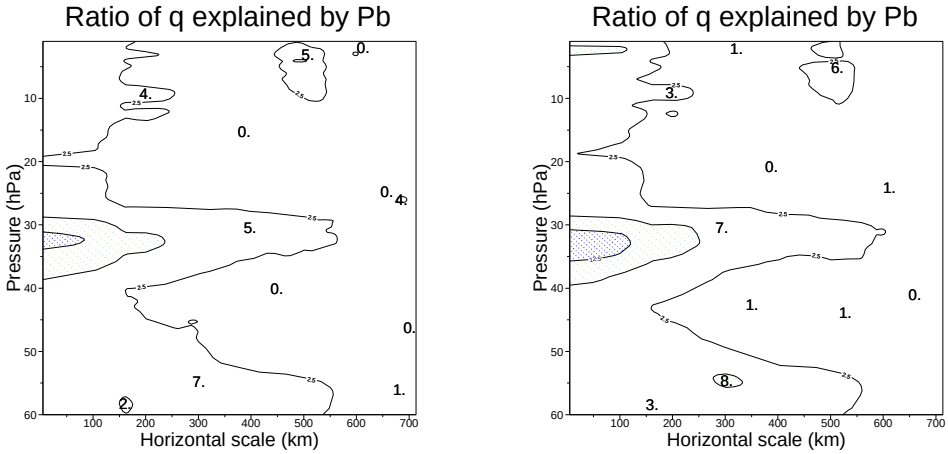

(c) (d)

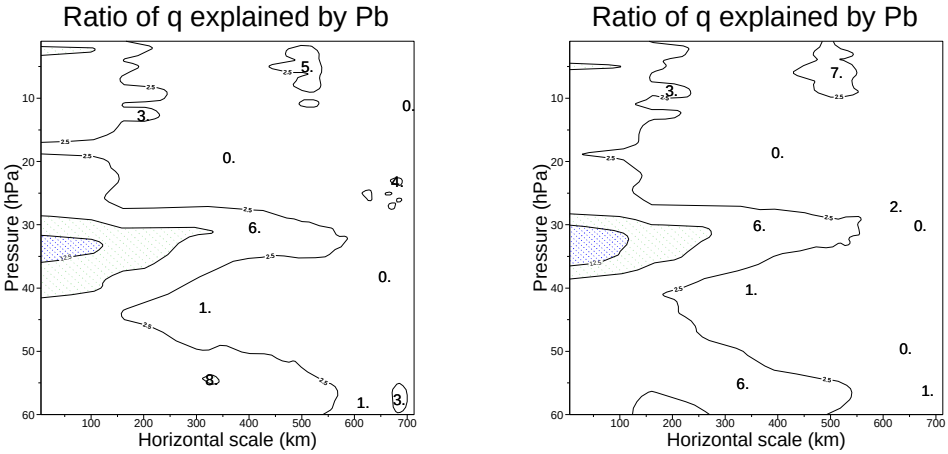

Figure 18: Percentage of the variance of specific humidity that is explained by balanced geopotential of 6 hour ALADIN/France forecast errors estimated by the second Summer ensemble, for all networks, for the model parameters: (a) 00UTC, (b) 06UTC, (c) 12UTC and (d) 18UTC.
l

(a) (b)

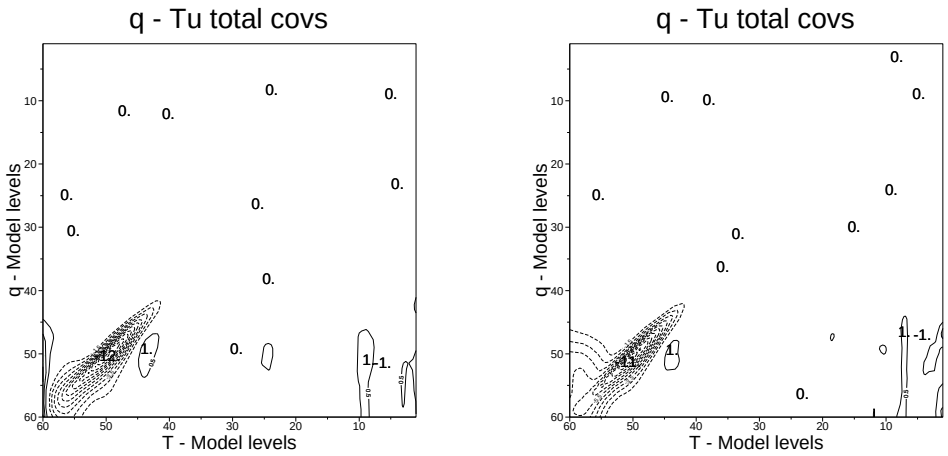

(c) (d)

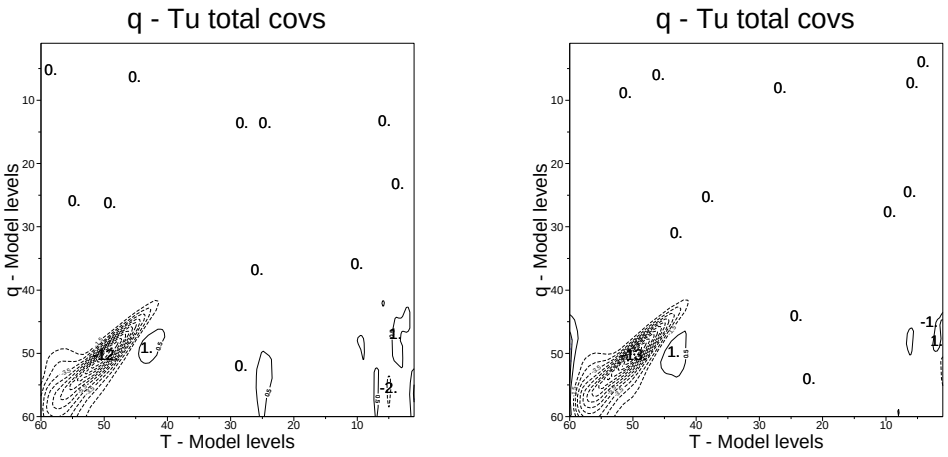

Figure 19: Mean vertical cross-covariance matrix between specific humidity and unbalanced temperature of 6 hour ALADIN/France forecast errors estimated by the second Winter ensemble for all networks: (a) 00UTC, (b) 06UTC, (c) 12UTC and (d) 18UTC.

(a) (b)

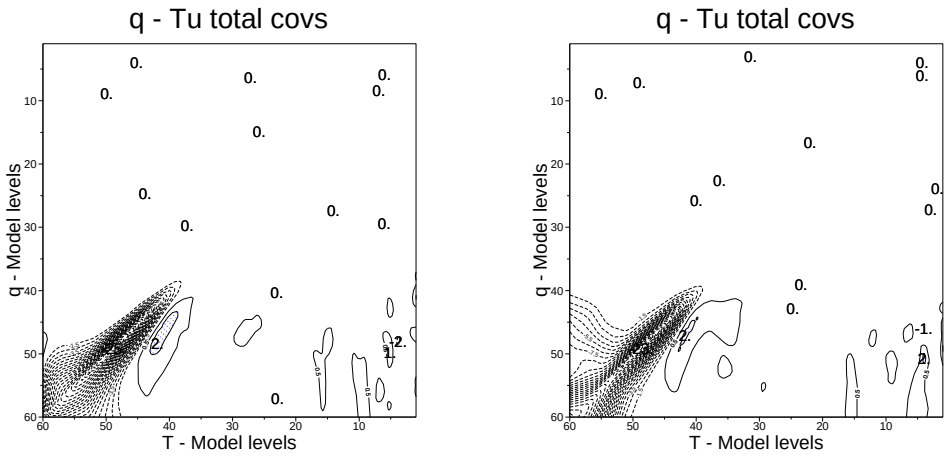

(c) (d)

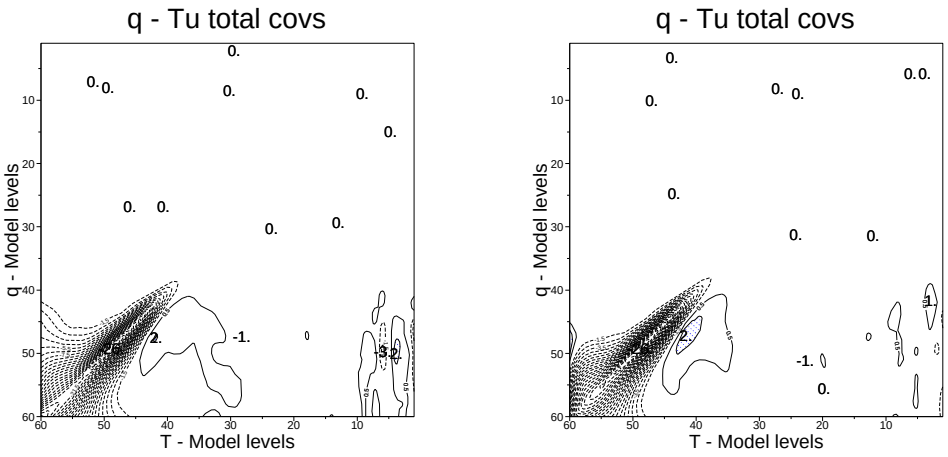

Figure 20: Mean vertical cross-covariance matrix between specific humidity and unbalanced temperature of 6 hour ALADIN/France forecast errors estimated by the second Summer ensemble for all networks: (a) 00UTC, (b) 06UTC, (c) 12UTC and (d) 18UTC.

(a) (b)

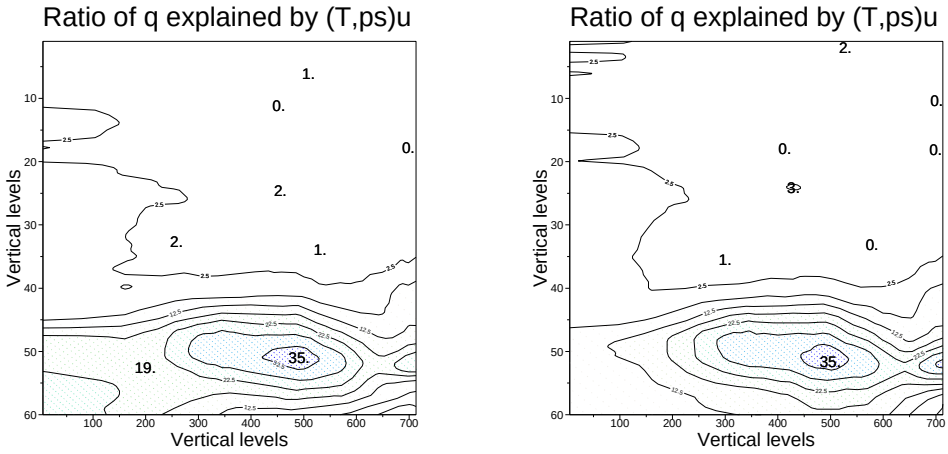

(c) (d)

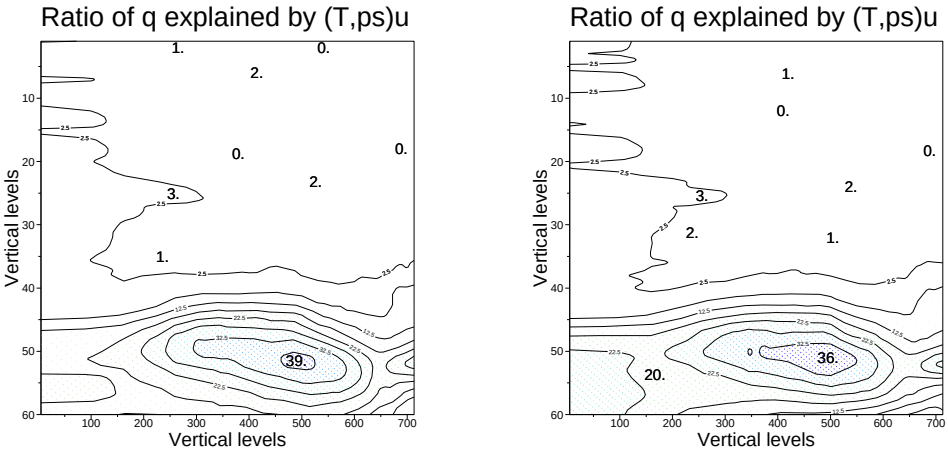

Figure 21: Percentage of the variance of specific humidity that is explained by unbalanced temperature and unbalanced surface pressure of 6 hour ALADIN/France forecast errors estimated by the second Winter ensemble for all the networks: (a) 00UTC, (b) 06UTC, (c) 12UTC and (d) 18UTC.

(a) (b)

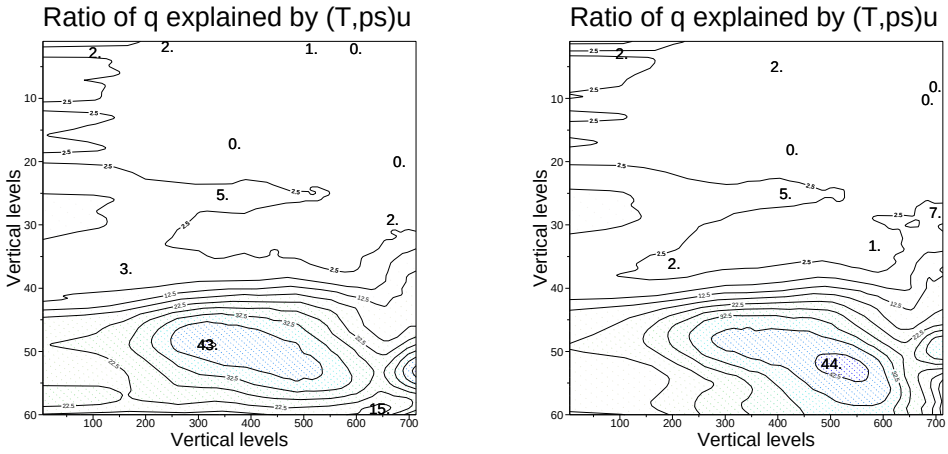

(c) (d)

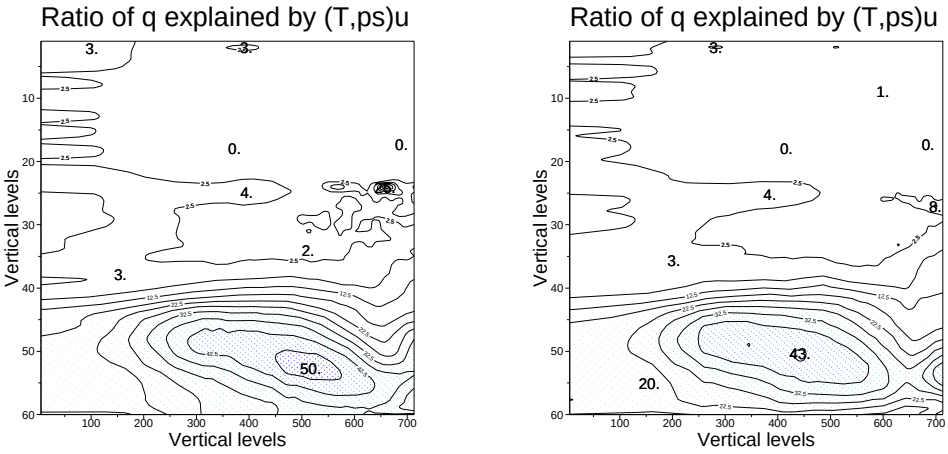

Figure 22: Percentage of the variance of specific humidity that is explained by unbalanced temperature and unbalanced surface pressure of 6 hour ALADIN/France forecast errors estimated by the second Summer ensemble for all the networks: (a) 00UTC, (b) 06UTC, (c) 12UTC and (d) 18UTC.

(a) (b)

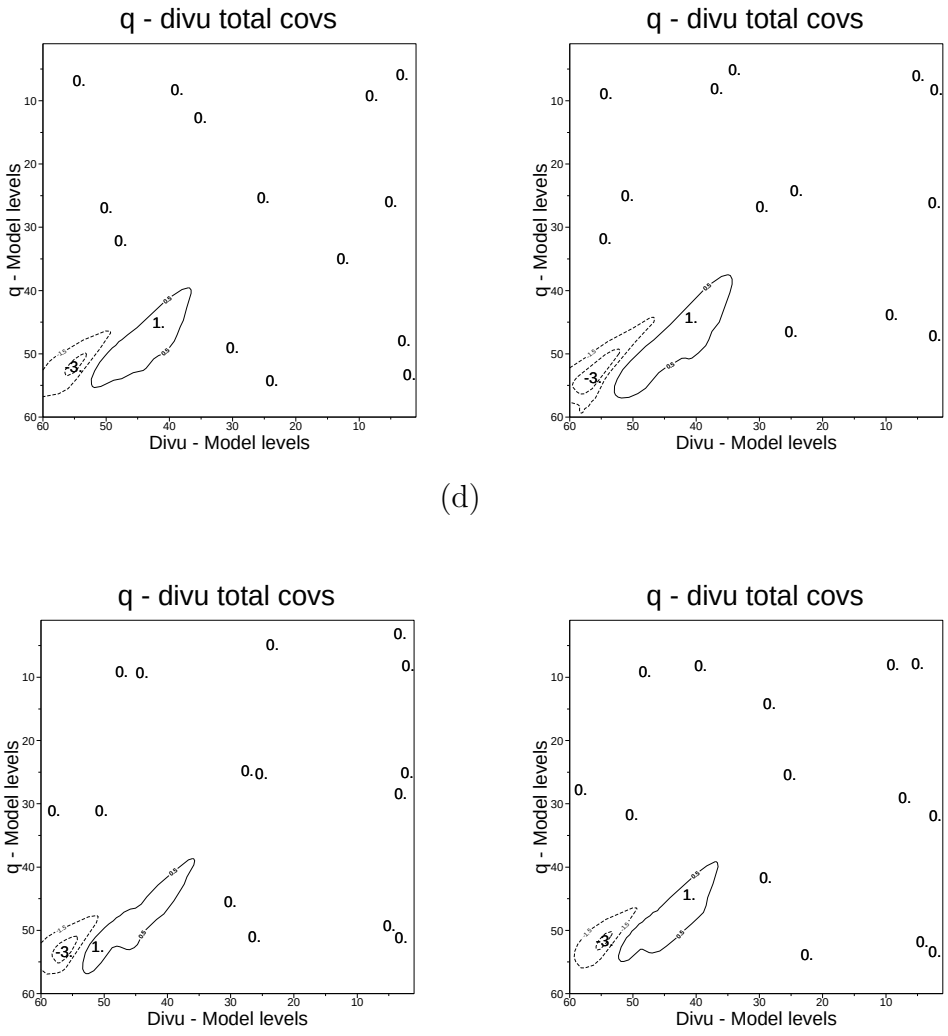

Figure 23: Mean vertical cross-covariance matrices between specific humidity and unbalanced divergence of 6 hour ALADIN/France forecast errors estimated by the second Winter ensemble, for all the networks: (a) 00UTC, (b) 06UTC, (c) 12UTC and (d) 18UTC.

(a) (b)

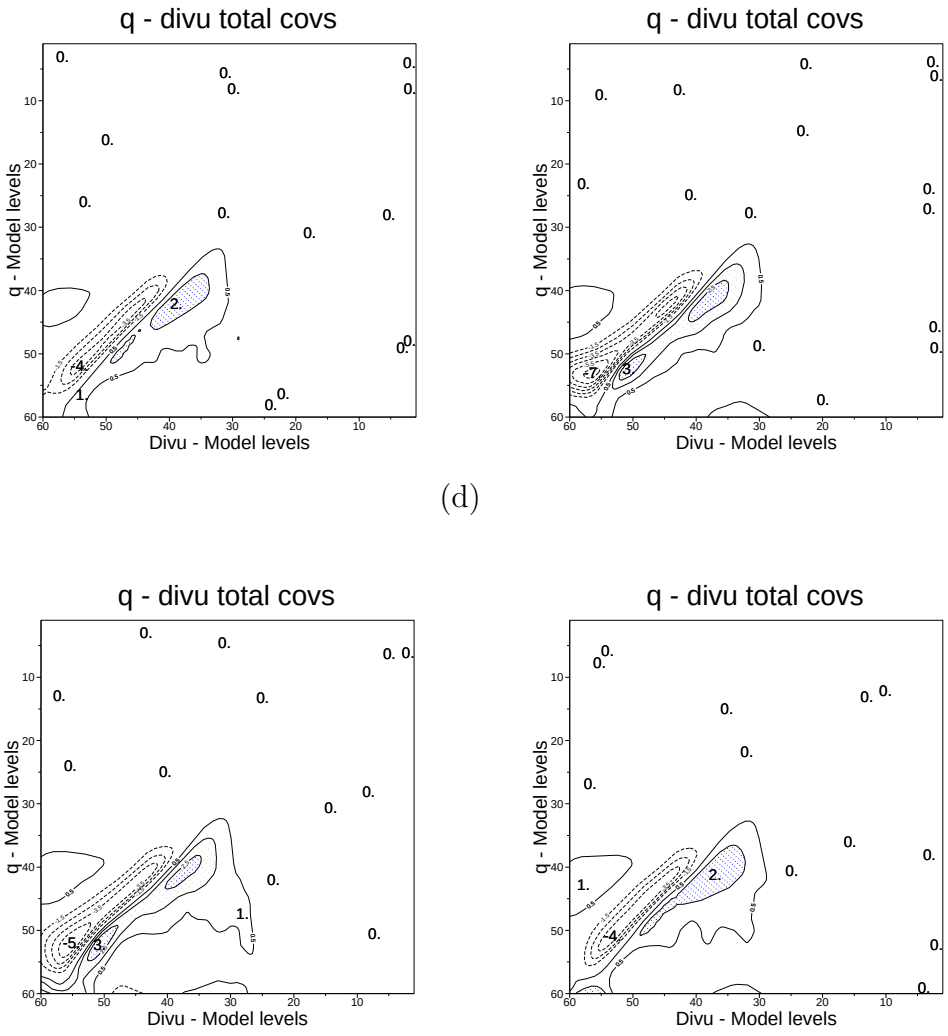

Figure 24: Mean vertical cross-covariance matrices between specific humidity and unbalanced divergence of 6 hour ALADIN/France forecast errors estimated by the first Summer ensemble, for all the networks: (a) 00UTC, (b) 06UTC, (c) 12UTC and (d) 18UTC.

(a) (b)

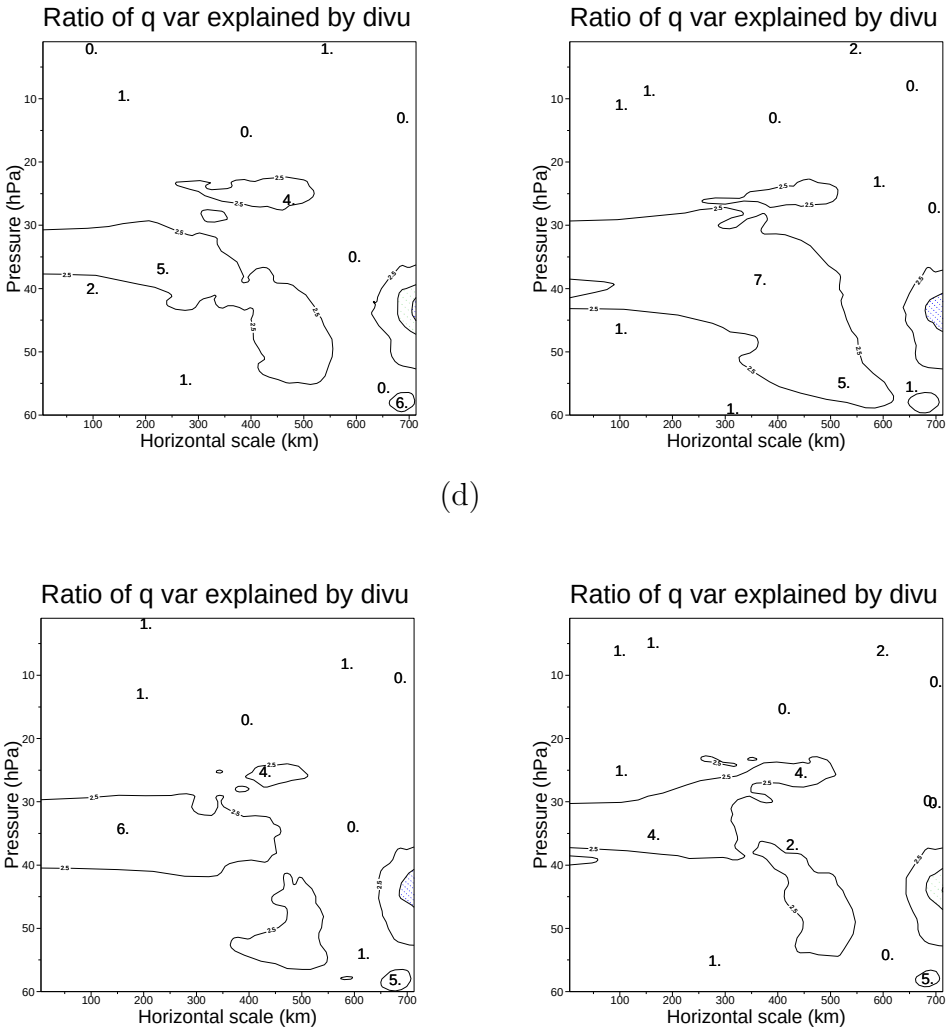

Figure 25: Percentage of the variance of specific humidity that is explained by unbalanced divergence of 6 hour ALADIN/France forecast errors estimated by the second Winter ensemble, as a fucntion of height and scale for all networks: (a) 00UTC, (b) 06UTC, (c) 12UTC and (d) 18UTC.

(a) (b)

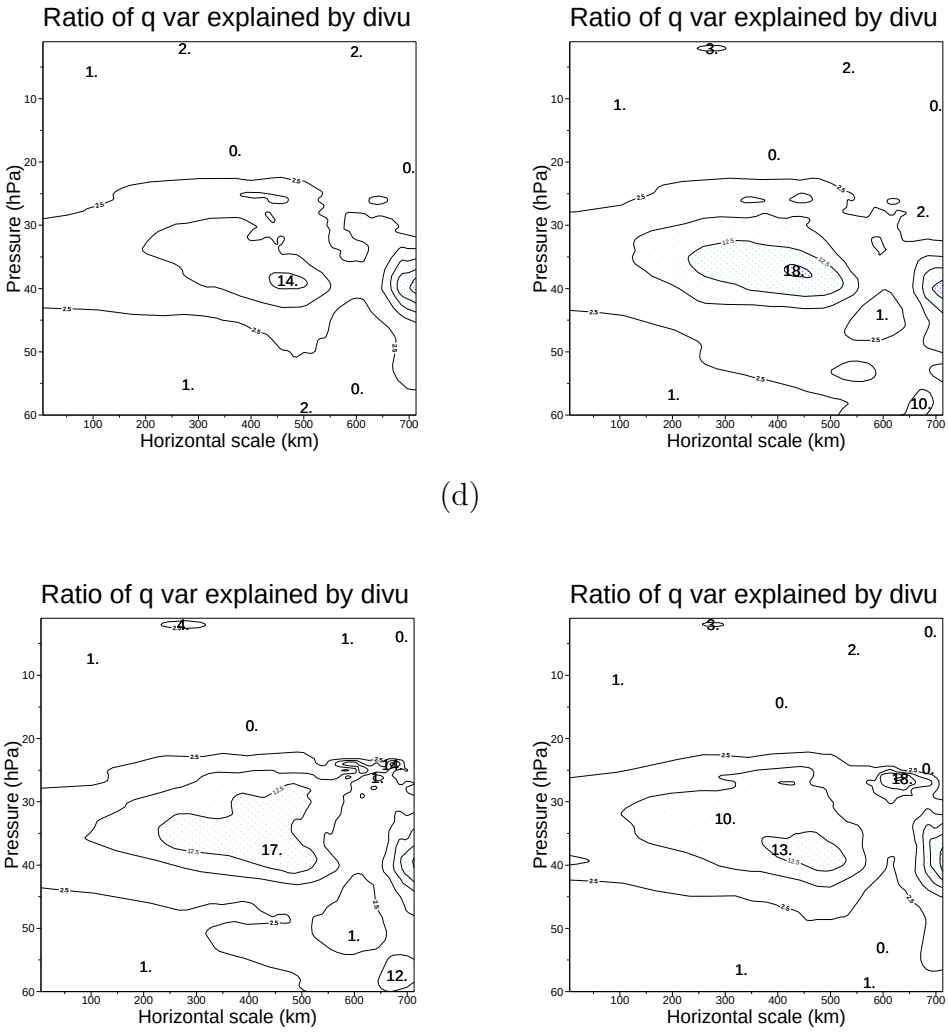

Figure 26: Percentage of the variance of specific humidity that is explained by unbalanced divergence of 6 hour ALADIN/France forecast errors estimated by the second Summer ensemble, as a fucntion of height and scale for all networks: (a) 00UTC, (b) 06UTC, (c) 12UTC and (d) 18UTC.

B Daily variation of cross-covariances

B.1 Mass-wind couplings

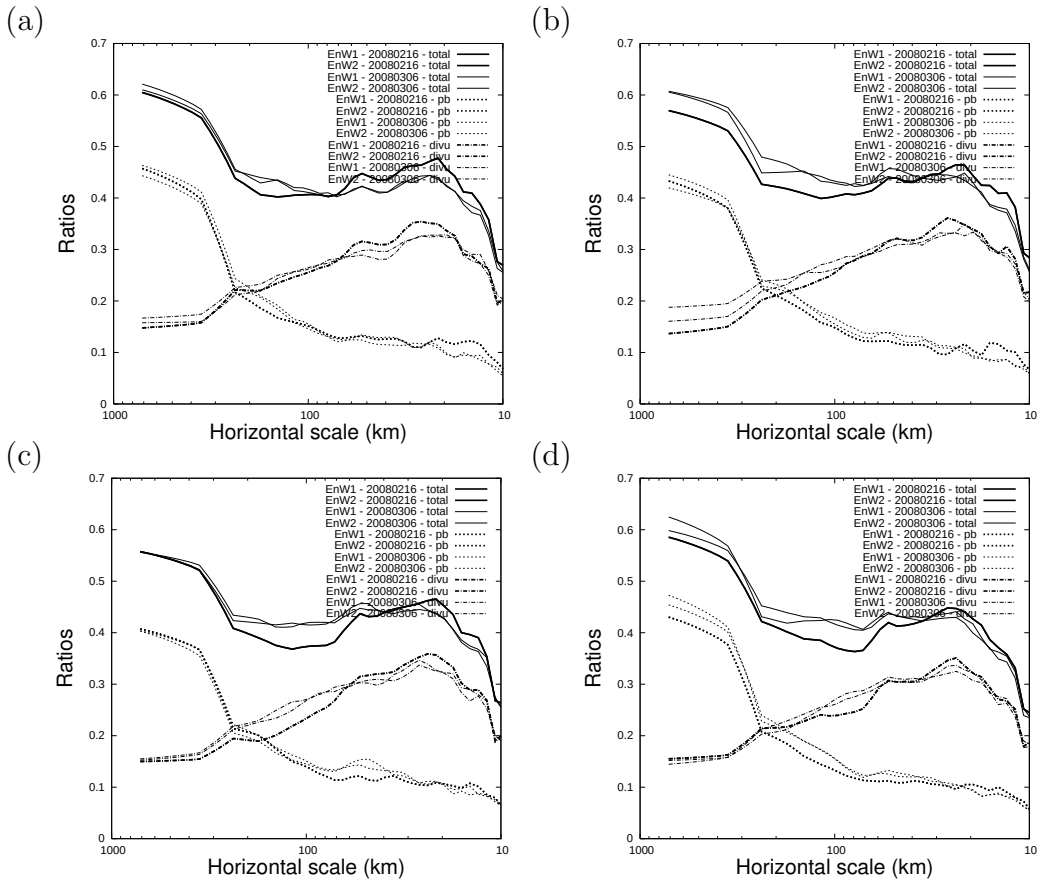

Figure 27: Vertical averages of the percentage of explained temperature variance of 6 hour ALADIN/France forecast errors estimated by the two Winter ensembles, for the two contrasting dates - 20080216 and 20080306 - and for all networks: (a) 00UTC, (b) 06UTC, (c) 12UTC and (d) 18UTC.

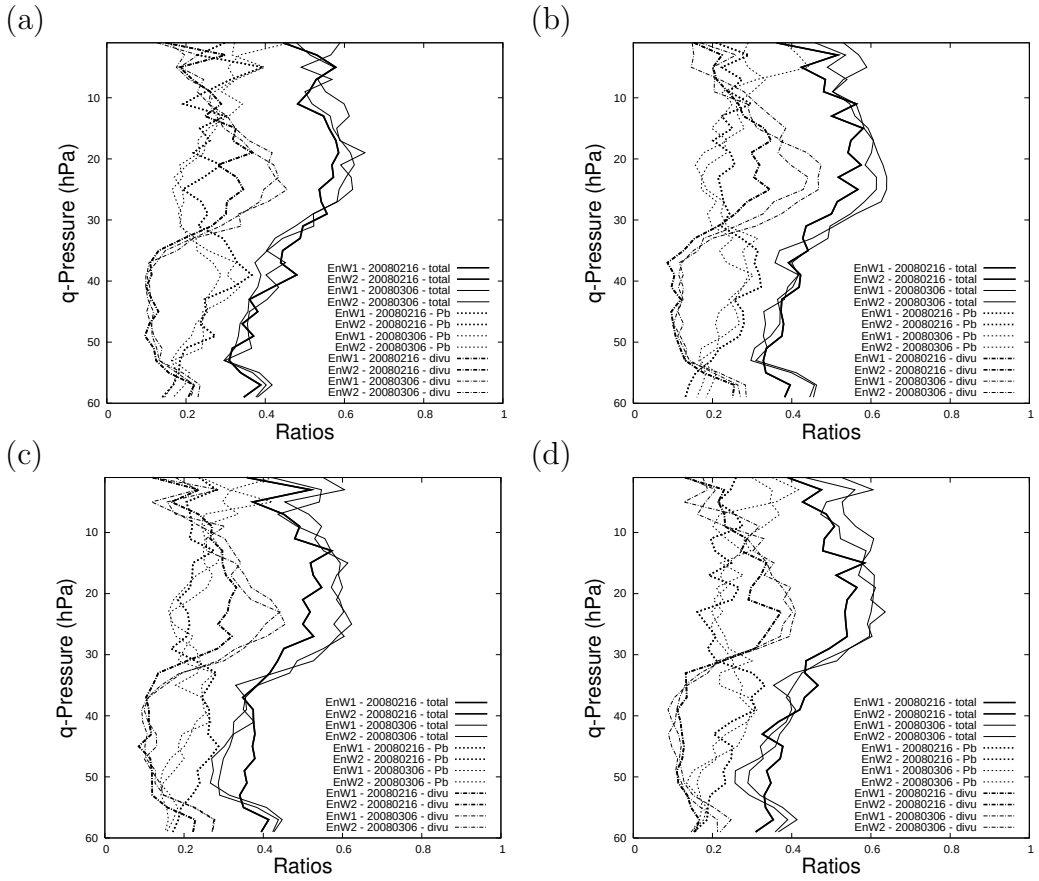

Figure 28: Vertical averages of the percentage of explained temperature variance of 6 hour ALADIN/France forecast errors estimated by the two Winter ensembles, for the two contrasting cases - 20080216 and 20080306 - and all networks: (a) 00UTC, (b) 06UTC, (c) 12UTC and (d) 18UTC.

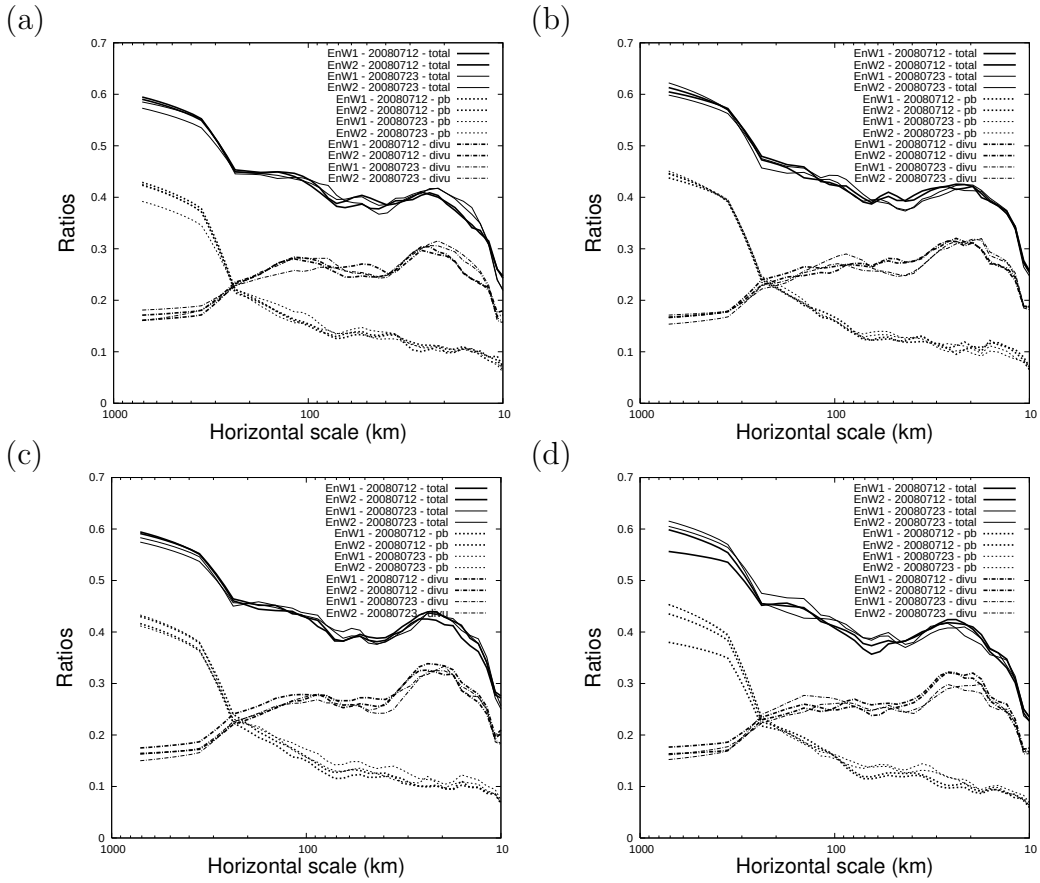

Figure 29: Vertical averages of the percentage of explained temperature variance of 6 hour ALADIN/France forecast errors estimated by the two Summer ensembles, for the contrasting cases - 20080712 and 20080723 - for all networks: (a) 00UTC, (b) 06UTC, (c) 12UTC and (d) 18UTC.

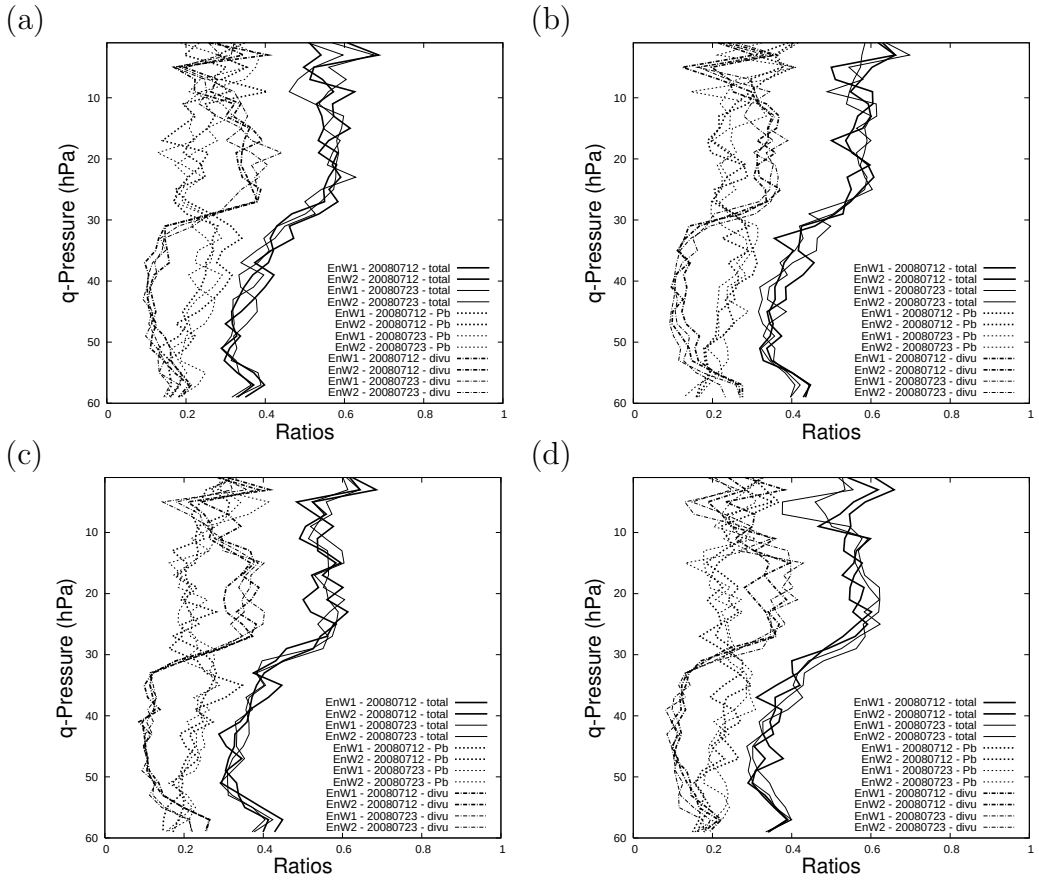

Figure 30: Vertical averages of the percentage of explained temperature variance of 6 hour ALADIN/France forecast errors estimated by the two Summer ensembles, for the two contrasting cases - 20080712 and 20080723 - and for all networks: (a) 00UTC, (b) 06UTC, (c) 12UTC and (d) 18UTC.

B.2 Couplings involving humidity

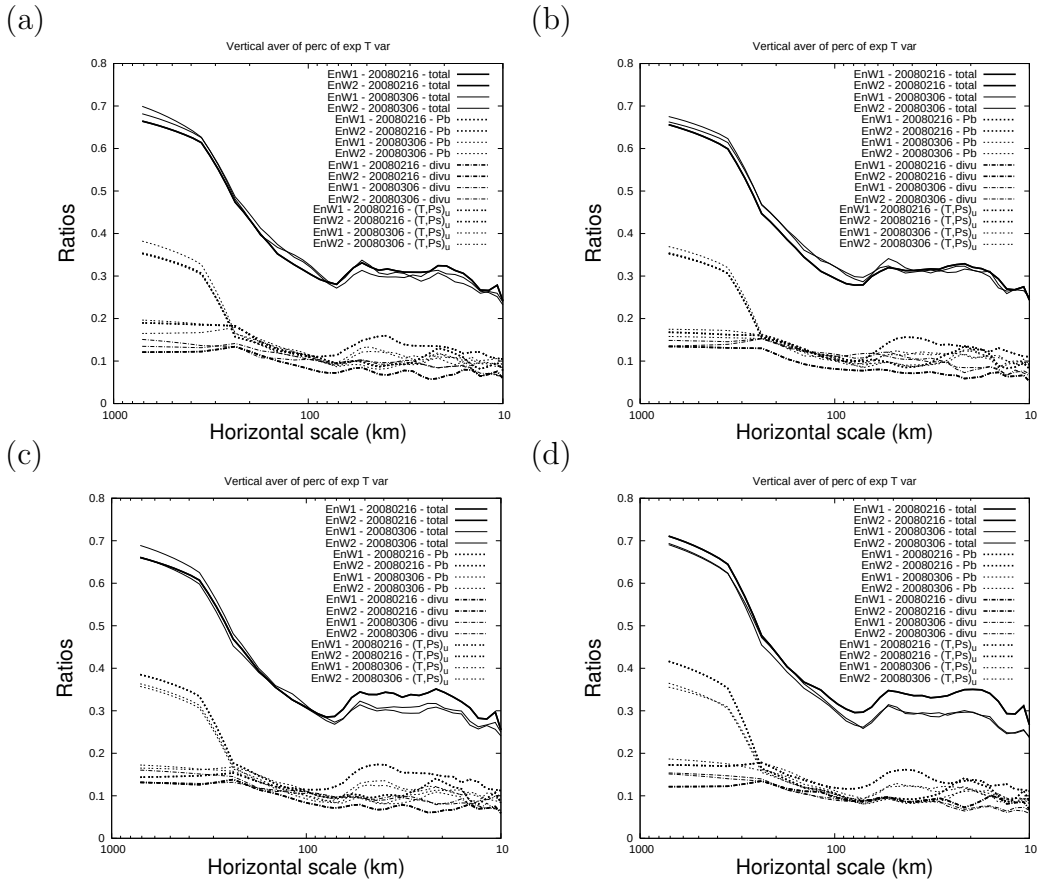

Figure 31: Vertical averages of the percentage of explained temperature variance of 6 hour ALADIN/France forecast errors estimated by the two Winter ensembles, for the two contrasting cases - 20080216 and 20080306 - and for all networks: (a) 00UTC, (b) 06UTC, (c) 12UTC and (d) 18UTC.

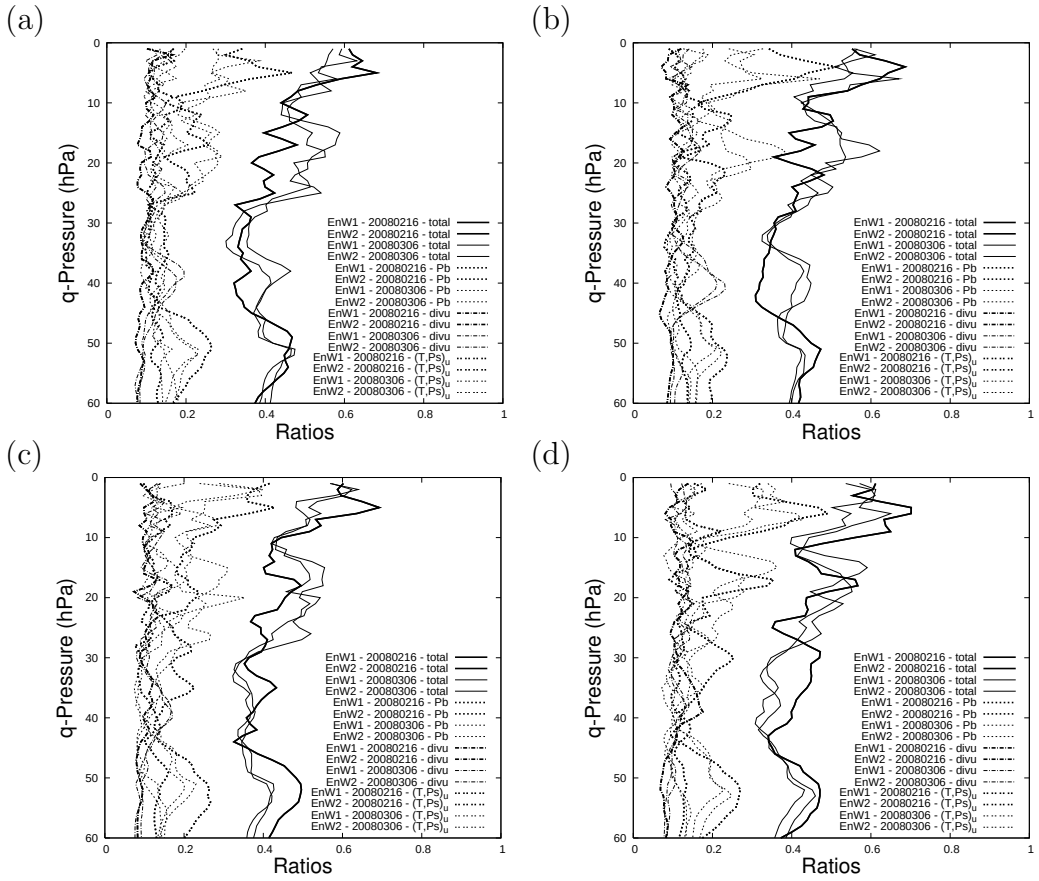

Figure 32: Vertical averages of the percentage of explained temperature variance of 6 hour ALADIN/France forecast errors estimated by the two Winter ensembles, for teh two contrasting cases - 20080216 and 20080306 - and for all networks: (a) 00UTC, (b) 06UTC, (c) 12UTC and (d) 18UTC.

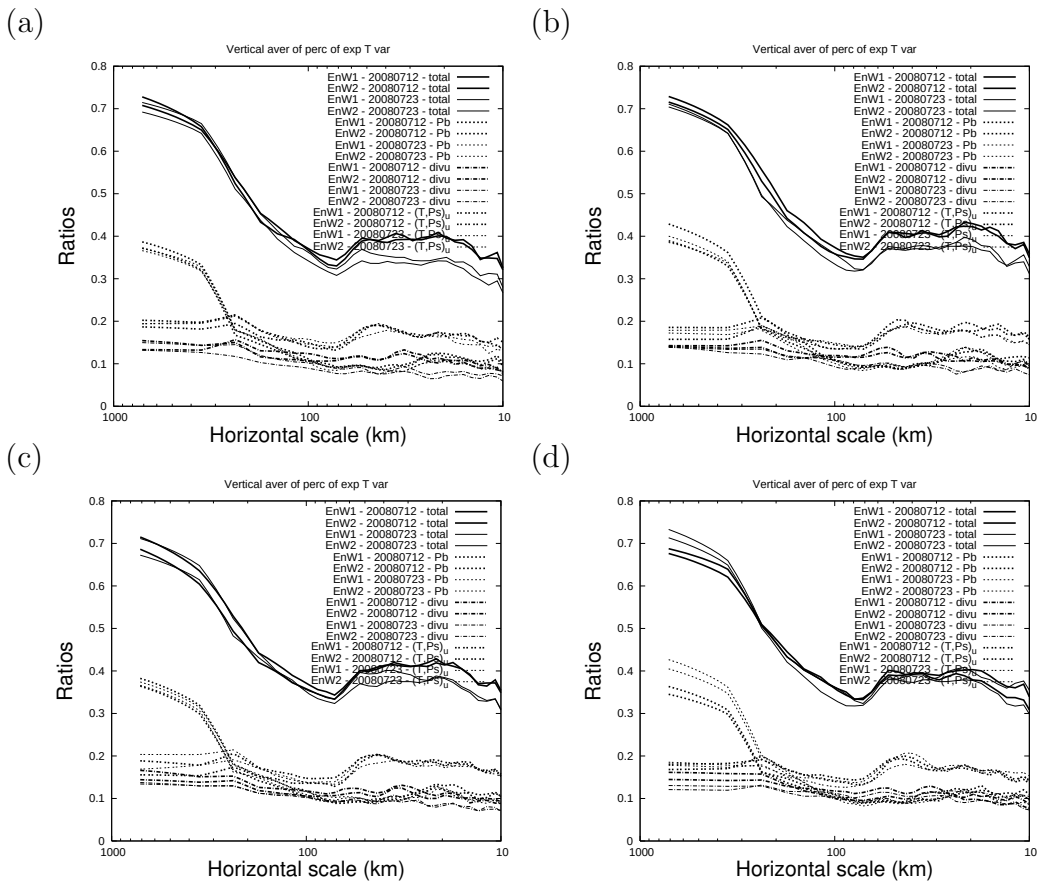

Figure 33: Vertical averages of the percentage of explained temperature variance of 6 hour ALADIN/France forecast errors estimated by the two Summer ensembles, for the two contrasting cases - 20080712 and 20080723 - and for all networks: (a) 00UTC, (b) 06UTC, (c) 12UTC and (d) 18UTC.

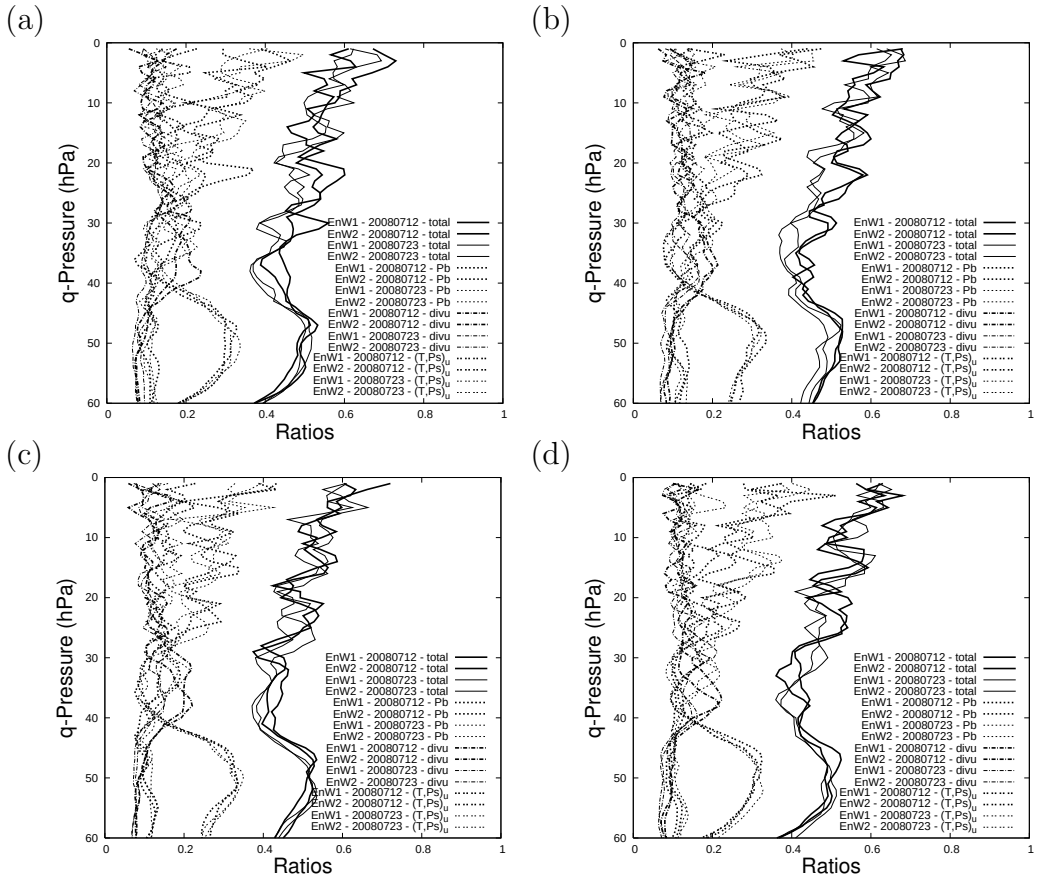

Figure 34: Vertical averages of the percentage of explained temperature variance of 6 hour ALADIN/France forecast errors estimated by the two Summer ensembles, for teh two contrasting cases - 20080712 and 20080723 - and for all networks: (a) 00UTC, (b) 06UTC, (c) 12UTC and (d) 18UTC.